crystals

MDPI

Article

# Local Vibrational Mode Analysis of $\pi$–Hole Interactions between Aryl Donors and Small Molecule Acceptors

**Seth Yannacone [1], Marek Freindorf [1], Yunwen Tao [1], Wenli Zou [2] and Elfi Kraka [1,*]**

[1] Department of Chemistry, Southern Methodist University, 3215 Daniel Avenue, Dallas, TX 75275, USA; syannacone@smu.edu (S.Y.); mfreindorf@smu.edu (M.F.); yunwent@smu.edu (Y.T.)
[2] Institute of Modern Physics, Northwest University, Xi'an 710127, China; zouwl@nwu.edu.cn
* Correspondence: ekraka@smu.edu; Tel.: +1-214-768-2611

Received: 6 June 2020; Accepted: 24 June 2020; Published: 30 June 2020


**Abstract:** 11 aryl–lone pair and three aryl–anion $\pi$–hole interactions are investigated, along with the argon–benzene dimer and water dimer as reference compounds, utilizing the local vibrational mode theory, originally introduced by Konkoli and Cremer, to quantify the strength of the $\pi$–hole interaction in terms of a new local vibrational mode stretching force constant between the two engaged monomers, which can be conveniently used to compare different $\pi$–hole systems. Several factors have emerged which influence strength of the $\pi$–hole interactions, including aryl substituent effects, the chemical nature of atoms composing the aryl rings/$\pi$–hole acceptors, and secondary bonding interactions between donors/acceptors. Substituent effects indirectly affect the $\pi$–hole interaction strength, where electronegative aryl-substituents moderately increase $\pi$–hole interaction strength. N-aryl members significantly increase $\pi$–hole interaction strength, and anion acceptors bind more strongly with the $\pi$–hole compared to charge neutral acceptors (lone–pair donors). Secondary bonding interactions between the acceptor and the atoms in the aryl ring can increase $\pi$–hole interaction strength, while hydrogen bonding between the $\pi$–hole acceptor/donor can significantly increase or decrease strength of the $\pi$–hole interaction depending on the directionality of hydrogen bond donation. Work is in progress expanding this research on aryl $\pi$–hole interactions to a large number of systems, including halides, CO, and $OCH_3^-$ as acceptors, in order to derive a general design protocol for new members of this interesting class of compounds.

**Keywords:** $\pi$–hole interaction; substituent effects; vibrational spectroscopy; local vibrational mode theory; direct measure for $\pi$–hole interaction strength; noncovalent interaction; hydrogen bonding

## 1. Introduction

The term '$\pi$–hole interaction' was coined by Murray and Politzer [1–4], and is described as a noncovalent interaction (NCI) between a region of positive electrostatic potential (ESP) located on a $\pi$–bond (i.e., a '$\pi$–hole') [5], and a lone–pair (lp) donor [6–8], anion [9,10], or other electron rich species [11,12]; where the $\pi$–hole is perpendicular to the molecular framework and electrons from the $\pi$–hole acceptor interact with an empty $\pi^*$ orbital of the donor. Some classic examples of $\pi$–hole interactions involving aryl groups include the benzene/hexafluorobenzene–water complexes, where an oxygen–lp interacts favorably with the center of the aromatic ring [13–20]. This special type of interaction has been identified in several important and highly relevant areas of modern chemical research, including drug targets [21,22], biological systems [23,24], and molecular crystals/solid state chemistry [25–30]. Interestingly, noble gases have recently been found capable of forming both $\sigma$– and $\pi$–hole interactions [31–33]. Ideal $\pi$–hole donors should contain heavier and more

polarizable atoms, as these properties improve accessibility, size, and positive ESP of a $\pi$–hole [34–37]. Electron withdrawing $\pi$–hole acceptors can also increase the positive ESP of the $\pi$–hole [38,39]. The main interaction energy terms describing $\pi$–hole interactions are: ion induced polarization and a permanent quadrupole moment ($Q_{zz}$) from the electrostatic forces [40–42]. Though there have been several recent theoretical and experimental studies on $\pi$–hole interactions [43–56], often the strength of these interactions is discussed in terms of bond lengths ($r$) or binding energies (BE)/dissociation energies (DE). However, these properties are not necessarily qualified as bond strength descriptors. There is an ample number of examples in which the shorter bond is not the stronger bond [57–59]. It is often assumed that BE or DE provide a measure of the intrinsic bond strength of the NCI in question. However this might not even be true in a qualitative sense, as BE and DE are cumulative properties; i.e., they are the sum of all interactions between the monomers, including long–range electrostatic interactions which may even involve the more remote atoms of the monomer [60]. Therefore, it is difficult to single out a specific interaction between atoms or groups of monomers; even computationally this can only be done in a qualitative way via an energy decomposition scheme, which leads to model dependent results [61–65]. In this situation, vibrational spectroscopy provides an excellent alternative for the description of the interactions between the monomers of a complex, and offers a platform for deriving a spectroscopic measure of complex stability. However, as has been frequently pointed out [60,66–69], any description of bond strength based on vibrational modes has to consider that normal vibrational modes are generally delocalized due to the coupling of the motions of the atoms within a molecule or complex [70–74]. Therefore, only decoupled local vibrational modes can serve as bond strength measurements, as was realized in the Local Vibrational Mode (LVM) theory originally formulated by Konkoli and Cremer [75–82]. Local mode stretching force constants ($k^a$) are directly related to the intrinsic strength of a bond, and therefore provide a unique measure of bond strength based on vibrational spectroscopy [83]. The local mode procedure was inspired by the isotopic substitution of McKean [84]. McKean found that if an XH fragment in a molecule is replaced by XD, a local X–D stretching mode may be detected in the IR spectrum, and therefore the force constant of the X–H or X–D stretching may be measured. This technology has been used to measure the force constants of many X–H bonds, but it cannot be extended to other systems due to the weak isotope effect. However, theoretical calculations are not limited to natural isotopes, allowing for isotopes of any mass to be "invented." The local mode procedure treats all the atoms which are not involved in a particular local mode as massless particles, so that they can effortless follow the local motion. For each local mode associated with an internal coordinate such as a bond length, bond angle, dihedral angle or puckering coordinate a unique local mode force constant, associated local mode mass and frequency can be obtained. So far, the LVM analysis has been successfully applied to characterize covalent bonds [59,66,83,85–88] and weak chemical interactions such as halogen [89–92], chalcogen [58,93,94], pnicogen [95–97], and tetrel interactions [98]; as well as hydrogen bonding (HB) [67,69,99–102]. For a comprehensive review the reader is referred to Ref. [80].

In this work, LVM theory is utilized to obtain a more accurate measurement of strength and the intrinsic nature of interactions between various aryl systems as $\pi$–hole donors and a number of small electron rich $\pi$–hole acceptors; where the $\pi$–hole either interacts with lp–electrons from a charge neutral acceptor, or an anionic acceptor species. A special inter–monomer LVM stretching force constant is utilized, which directly assesses the strength of the $\pi$–hole$\cdots\pi$–hole acceptor interaction. Based on this special inter–monomer $k^a$ measure, recently and for the first time, the strength of metal–ring interactions in a series of actinide sandwich compounds was quantified [103], and a nonclassical HB involving a BH$\cdots\pi$ interaction was identified [104,105]. Burianova et al. concurrently verified this type of nonclassical HB involving a BH$\cdots\pi$ interaction both experimentally and theoretically while performing a mechanistic study involving the nucleophilic addition of hydrazines, hydrazides, and hydrazones to C≡N groups of boron–based clusters [106].

The current work investigates the interactions of $\pi$–hole acceptors $H_2O$, HCN, $NH_3$, and $NO_3^-$, with the following aromatic $\pi$–hole donors: $C_6F_6$, $C_6F_5H$, $C_6F_4H_2$, $C_6F_3H_3$, $N_3C_3H_3$, $N_3C_3F_3$,

and $N_4C_2H_2$ (see Figure 1). Original theoretical works of similar nature date back to 1997, when Alkorta et al. investigated the effects of F–substitution on reactivity of the aromatic rings in systems where small electron-donating molecules interact with the $\pi$–clouds of benzene and hexafluorobenzene [107]. An extension of this work was reported in 2002, which included a larger array of aromatics and benzene derivatives and several negatively charged electron donors [108]. Simultaneously, a similar phenomenon was reported involving 1,3,5–triazine derivatives interacting with $F^-$, $Cl^-$, and azide ($N_3$) [109], and a computation study was combined with crystallographic evidence to confirm such interactions can favorably occur [110].

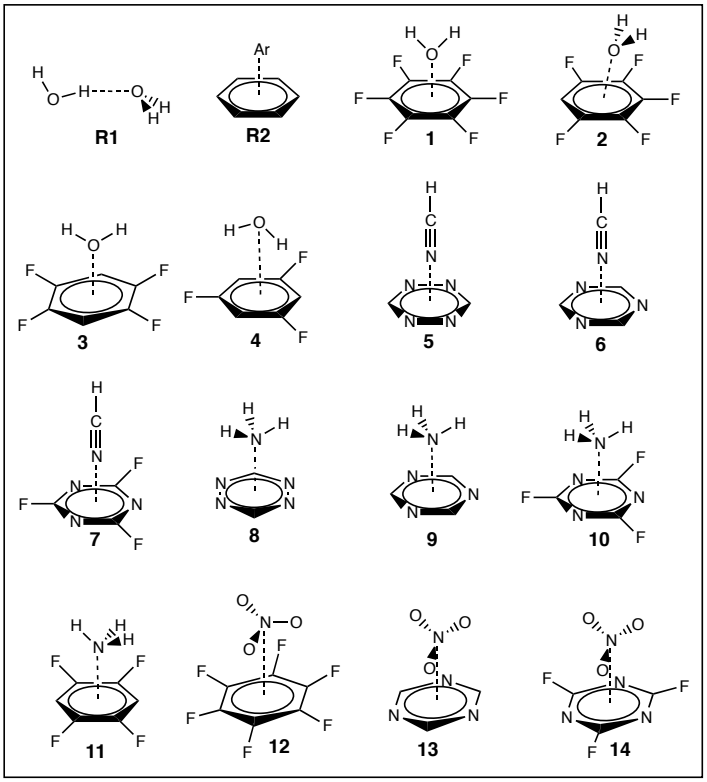


**Figure 1.** Schematic of the two references systems, **R1** and **R2**, and $\pi$–hole systems **1–14** studied in this work showing molecular geometries of each system; calculated at the $\omega$B97X–D/aug–cc–pVTZ level of theory.

## 2. Computational Methods

DFT was utilized to optimize molecular geometries, calculate stationary point normal mode vibrational frequencies ($\omega_\mu$), LVM frequencies ($\omega^a$), $k^a$ [75,78,79], and Natural Bond Orbital (NBO) charges. Calculations were carried out at the $\omega$B97X–D/aug–cc–pVTZ level of theory with tight convergence criteria and superfine integration grid [111–116]. All stationary points were confirmed to be minima by absence of imaginary $\omega_\mu$. Calculated and experimental vibrational frequencies of the $H_2O\cdots C_6F_6$ [117] system were used to gauge the accuracy of several model chemistries (see Tables 1 and 2). Theoretical vibrational spectroscopy was utilized to quantify the intrinsic strength of $\pi$–hole interactions in this work. Normal vibrational modes do not give direct measurements of bond strength because of electronic and mass coupling. This results in delocalization of the normal modes in most cases. The electronic coupling is eliminated by solving the Wilson equation of spectroscopy [118] and transforming to normal coordinates. Konkoli and Cremer found that mass coupling can be removed by solving a mass–decoupled equivalent of the Wilson equation, which leads to LVMs. LVMs are associated with internal coordinates: bond length, bond angle, or dihedral angle [76], and lead

to a direct relationship between the intrinsic strength of a bond and its $k^a$ value [83]. For the first time, this theory is applied to $\pi$–hole interactions. LVM analysis was computed with the program COLOGNE2018 [119]. NBO populations were calculated using NBO6 [120–122]. Calculations of $\rho(\mathbf{r}_{CCP})$ and $\nabla^2\rho(\mathbf{r}_{CCP})$ were performed with the AIMAll program [123,124]. All DFT calculations were made with GAUSSIAN16 [125].

**Table 1.** Comparison of experimental *exp* normal mode vibrational frequencies $\omega_{exp}$, with theoretical normal mode vibrational frequencies $\omega_\mu$ for **1** computed at the $\omega$B97X–D/aug–cc–pVTZ, $\omega$B97X–D/aug–cc–pVQZ, $\omega$B97X–D/def2–TZVPP, MP2/aug–cc–pVTZ , and MP2/def2–TZVPP levels of theory.

| Mode | *exp* [117] | $\omega$B97X–D/ aug–cc–pVTZ | $\omega$B97X–D/ aug–cc–pVQZ | $\omega$B97X–D/ def2–TZVPP | MP2/ aug–cc–pVTZ | MP2/ def2–TZVPP |
|---|---|---|---|---|---|---|
| $H_2O$ $\nu_3$ (asymmetric stretch) | 3723.0 | 3811.0 (−2.3) | 3821.4 (−2.6) | 3822.2 (−2.6) | 3745.8 (−0.6) | 3769.9 (−1.2) |
| $H_2O$ $\nu_1$ (symmetric stretch) | 3632.0 | 3710.3 (−2.1) | 3722.4 (−2.4) | 3722.2 (−2.4) | 3629.7 (0.1) | 3655.8 (−0.7) |
| $H_2O$ $\nu_2$ (bend) | 1607.0 | 1570.2 (2.3) | 1572.7 (2.2) | 1568.7 (2.4) | 1558.2 (3.1) | 1570.1 (2.3) |
| $C_6H_6$ $\nu_{12}$ (C−C stretch) | 1536.0 | 1511.4 (1.6) | 1510.2 (1.7) | 1509.7 (1.7) | 1489.2 (3.1) | 1495.5 (2.7) |
| $C_6H_6$ $\nu_{13}$ (C−F stretch) | 999.0 | 991.8 (0.7) | 991.5 (0.8) | 990.0 (0.9) | 971.4 (2.8) | 976.1 (2.3) |

$\omega_{exp}$ and $\omega_\mu$ are reported in $cm^{-1}$ and errors are given as % with respect to *exp* in parentheses next to each $\omega_\mu$. Scaling factors are as follows: 0.957 ($\omega$B97X–D/aug–cc–pVTZ), 0.957 ($\omega$B97X–D/aug–cc–pVQZ), 0.955 ($\omega$B97X–D/def2-TZVPP), 0.953 (MP2/aug–cc–pVTZ), and 0.952 (MP2/def2-TZVPP) [126–132].

**Table 2.** Comparison of local vibrational mode LVM data for $\pi$–hole system **1**, where O···$C_6$ (acceptor···donor) represents the pure $\pi$–hole interaction between the acceptor O–atom and the geometric center of the C–atoms comprising the six–membered ring, O···$C_6F_6$ denotes similar as above but includes the six F–substituents of the $\pi$–hole donor, H···$C_6$ denotes one acceptor H–atom interacting with the geometric center of the six donor C–atoms, and H···$C_6F_6$ represents the aforementioned interaction with inclusion of the aryl F–substituents.

| Parameter | *r* | $k^a$ | $\omega^a$ |
|---|---|---|---|
| $\omega$B97X–D/aug–cc–pVTZ | | | |
| O···$C_6$ | 3.121 | 0.090 | 108.1 |
| O···$C_6F_6$ | 3.116 | 0.087 | 100.2 |
| H···$C_6$ | 3.780 | 0.021 | 187.1 |
| H···$C_6F_6$ | 3.775 | 0.020 | 185.7 |
| $\omega$B97X–D/aug–cc–pVQZ | | | |
| O···$C_6$ | 3.130 | 0.082 | 103.2 |
| O···$C_6F_6$ | 3.125 | 0.080 | 95.7 |
| H···$C_6$ | 3.787 | 0.020 | 185.6 |
| H···$C_6F_6$ | 3.782 | 0.020 | 184.1 |
| MP2/aug–cc–pVTZ | | | |
| O···$C_6$ | 2.981 | 0.087 | 106.3 |
| O···$C_6F_6$ | 2.974 | 0.084 | 98.1 |
| H···$C_6$ | 3.654 | 0.023 | 197.7 |
| H···$C_6F_6$ | 3.646 | 0.023 | 195.8 |

bond lengths *r* are given in Å, LVM force constants $k^a$ in mdyn/Å, and units for LVM frequencies $\omega^a$ are $cm^{-1}$.

Figure 2 illustrates how the special force constant $k^a$ is defined for the special case of the $\pi$–hole interaction involving a six–membered ring as $\pi$–hole donor. $k^a$ is defined via the direct interaction between the central O– or N–atom of the $\pi$–hole acceptor (position $X_1$ in Figure 2) and the geometric

center of the six atoms composing the aryl ring of the $\pi$–hole donor ($X_2$ in Figure 2). A key feature of the LVM methodology is that the $\pi$–hole need not be at the $X_2$ geometric center of the ring. If this is the case, and the acceptor atom at $X_1$ is collinear with $X_2$ and the $\pi$–hole, the value of $k^a$ will not change because the local modes of $X_1 \cdots X_2$ and $X_1 \cdots \pi$–hole are normalized in the LVM theory formalism. In systems **R2**, **1–4** and **11–12**, the ring atoms are all carbon; whereas in systems **6–7**, **9–10**, and **13–14**, three N–atoms and three C–atoms are incorporated into the ring structure. In systems **5** and **8**, the six–membered rings are composed of four N–atoms and two C–atoms.

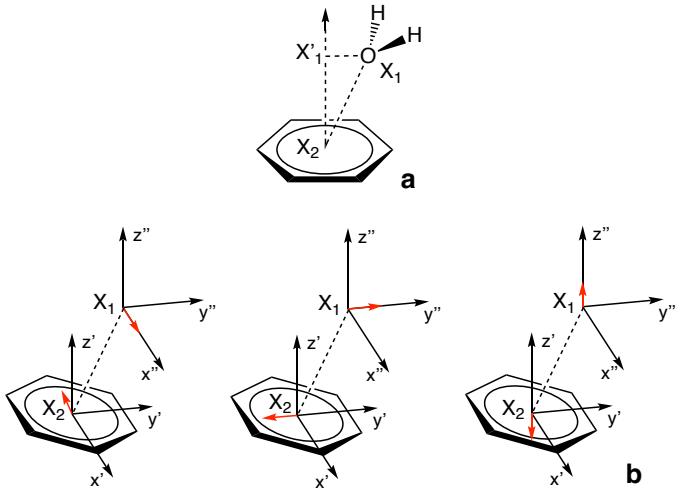


**Figure 2.** Schematic of how the special LVM force constant $k^a$ is defined for the $\pi$–hole interaction involving a six–membered aromatic ring as $\pi$–hole donor, where $X_1$ is the location of the central atom of the acceptor molecule interacting directly with the $\pi$–hole located at $X_2$; shown is complex **2**.

## 3. Results/Discussion

### *3.1. Discussion of Model Chemistry*

Table 1 shows experimental (*exp*) normal mode frequencies ($\omega_{exp}$) and theoretical normal mode frequencies ($\omega_\mu$) for the water-hexafluorobenzene dimer (system **1**). Theoretical $\omega_\mu$ were computed using Møller–Plesset perturbation theory of second order (MP2) and the $\omega$B97X–D functional combined with aug–cc–pVTZ, aug–cc–pVQZ, and def2–TZVPP basis sets. In addition, scaling factors were applied to theoretical frequencies to correct for approximations to the full electronic configuration interaction and the harmonic approximation to the Morse potential [126–132]. In parentheses directly to the right of each theoretical frequency, are % error values calculated with respect to *exp*. It turns out that $\omega$B97X–D/aug–cc–pVTZ calculations were in closest agreement with *exp*. MP2 calculations performed best for the highest frequencies, but were less accurate for low frequencies. The opposite is true of calculations carried out using $\omega$B97X–D. The use of the def2-TZVPP basis set was computationally more efficient, but the aug–cc–pVTZ basis set significantly improved accuracy.

Table 2 compares LVM data calculated at the $\omega$B97X–D/aug–cc–pVTZ, $\omega$B97X–D/aug–cc–pVQZ, and MP2/aug–cc–pVTZ levels of theory for $\pi$–hole system **1**, where $O \cdots C_6$ denotes the pure $\pi$–hole interaction between the acceptor O–atom and the geometric center of the C–atoms composing the six–membered ring (acceptor···donor). $O \cdots C_6F_6$ is very similar to the interaction just described, except in this case the six F–substituents are included. $H \cdots C_6$ denotes the interaction between one acceptor H–atom and the geometric center of the six donor C–atoms; whereas $H \cdots C_6F_6$ denotes a similar interaction, but with the six F–substituents included (analogous to the $O \cdots C_6/O \cdots C_6F_6$ comparison). The $\pi$–hole interactions in the remainder of this work are defined using the first notation

($O\cdots C_6$) in Table 2: the pure $\pi$–hole interaction between the central acceptor atom and the geometric center of the donor six–membered ring, not including aryl substituent atoms.

In comparison with the $\omega$B97X–D/aug–cc–pVTZ calculations, adding a larger basis set (aug–cc–pVQZ quality) resulted in a modest $r$ increase of 0.009 Å and a slight decrease in $k^a$ of 0.008 mdyn/Å. On the other hand, MP2/aug–cc–pVTZ results gave significantly shorter $r$ (by 0.140 Å and 0.149 Å), slightly weaker bond strength (by 0.003 mdyn/Å) compared to $\omega$B97X–D/aug–cc–pVTZ, and slightly stronger bond strength (by 0.005 mdyn/Å) compared to $\omega$B97X–D/aug–cc–pVQZ. This result is erratic in the case of MP2/aug–cc–pVTZ. The $\omega$B97X–D/aug–cc–pVQZ level of theory has large computational cost with small increase of accuracy compared to $\omega$B97X–D/aug–cc–pVTZ. Therefore, we have chosen in this study the $\omega$B97X–D/aug–cc–pVTZ level of theory as a compromise between accuracy and computational efficiency. Note that for the remainder of this work, the terms '$k^a$' and 'bond strength' are used interchangeably. In addition, the term secondary bonding interaction (SBI) refers to any interaction between a single atom of the acceptor molecule and a single atom of the donor molecule which contains a physically meaningful LVM.

### *3.2. Overall Findings and General Trends*

Table 3 summarizes the LVM data of the $\pi$–hole interactions in **1–14** and two reference NCIs: **R1** (water dimer) and **R2** ($Ar\cdots C_6H_6$). Figure 3 (top) shows molecular geometry of each system, $r$ (shown in green), $k^a$ (blue), $\omega^a$ (red), and symmetry point group (black) for **R1**, **R2**, and **1–14**. **R1** and **R2** have been incorporated to provide a frame of reference from well characterized compounds: The $H_2O$ dimer represents complex containing a strong HB with non-negligible covalent character, and $Ar\cdots C_6H_6$ represents a weak NCI [133]. Also in Figure 3 (bottom), selected NBO charges are given, where charges in green represent C–atoms, O–atomic charges are red, H–atomic charges are black, N–atomic charges are blue, and F–atomic charges are light blue. Bond length $r$ and NBO charge on the acceptor O and N–atoms are plotted with respect to $k^a$ in Figure 4a and Figure 4b, respectively. Shown as red plot points are interactions where $H_2O$ is the acceptor (**1–4**), light blue points represent HCN acceptor systems (**5–7**), in green are $NH_3$ (**8–11**), blue points are the $NO_3^-$ anion–$\pi$–hole interactions (**12–14**), and black points indicate **R1** and **R2**. This color convention is maintained in the subsequent plots.

**Table 3.** Summary of LVM data: $\pi$–hole interaction distances $r$, $k^a$, $\omega^a$, charge transfer CT, and BSSE counterpoise corrected binding energies BE.

| # | System | Point Group | $r$ | $k^a$ | $\omega^a$ | CT lp→ $\pi$–hole | BE |
|---|---|---|---|---|---|---|---|
| **R1** | $H_2O\cdots HOH$ | $C_s$ | 1.936 | 0.171 | 553.3 | −9.08 | −4.98 |
| **R2** | $Ar\cdots C_6H_6$ | $C_{2v}$ | 3.620 | 0.072 | 69.0 | −0.10 | −0.92 |
| **1** | $H_2O\cdots C_6F_6$ | $C_{2v}$ | 3.121 | 0.090 | 108.1 | −10.29 | −2.57 |
| **2** | $H_2O\cdots C_6F_5H$ | $C_s$ | 3.193 | 0.051 | 81.3 | −7.72 | −2.10 |
| **3** | $H_2O\cdots C_6F_4H_2$ | $C_{2v}$ | 3.226 | 0.107 | 117.6 | −5.66 | −1.52 |
| **4** | $H_2O\cdots C_6F_3H_3$ | $C_s$ | 3.359 | 0.086 | 105.5 | −1.75 | −2.03 |
| **5** | $HCN\cdots N_4C_2H_2$ | $C_{2v}$ | 3.047 | 0.090 | 113.3 | −30.99 | −2.65 |
| **6** | $HCN\cdots N_3C_3H_3$ | $C_{3v}$ | 3.154 | 0.051 | 85.2 | −19.93 | −1.75 |
| **7** | $HCN\cdots N_3C_3F_3$ | $C_{3v}$ | 2.989 | 0.076 | 104.0 | −45.02 | −4.05 |
| **8** | $H_3N\cdots N_4C_2H_2$ | $C_s$ | 3.062 | 0.125 | 133.7 | −16.07 | −3.87 |
| **9** | $H_3N\cdots N_3C_3H_3$ | $C_{3v}$ | 3.170 | 0.144 | 143.7 | −9.50 | −2.54 |
| **10** | $H_3N\cdots N_3C_3F_3$ | $C_{3v}$ | 3.026 | 0.185 | 162.8 | −2.80 | −5.37 |
| **11** | $H_3N\cdots C_6F_4H_2$ | $C_s$ | 3.298 | 0.070 | 100.9 | −8.24 | −2.03 |
| **12** | $[O_3N\cdots C_6F_6]^-$ | $C_{3v}$ | 3.078 | 0.228 | 181.7 | −5.83 | −12.00 |
| **13** | $[O_3N\cdots N_3C_3H_3]^-$ | $C_{3v}$ | 3.128 | 0.169 | 155.7 | −6.32 | −6.03 |
| **14** | $[O_3N\cdots N_3C_3F_3]^-$ | $C_{3v}$ | 2.955 | 0.276 | 198.6 | −11.31 | −13.03 |

Calculated at $\omega$B97X–D/aug–cc–pVTZ level of theory. Units for reported data as follows: $r$ in Å, $k^a$ in mdyn/Å, $\omega^a$ in $cm^{-1}$, CT in milli-electron ($m_e$), and BE in kcal/mol.

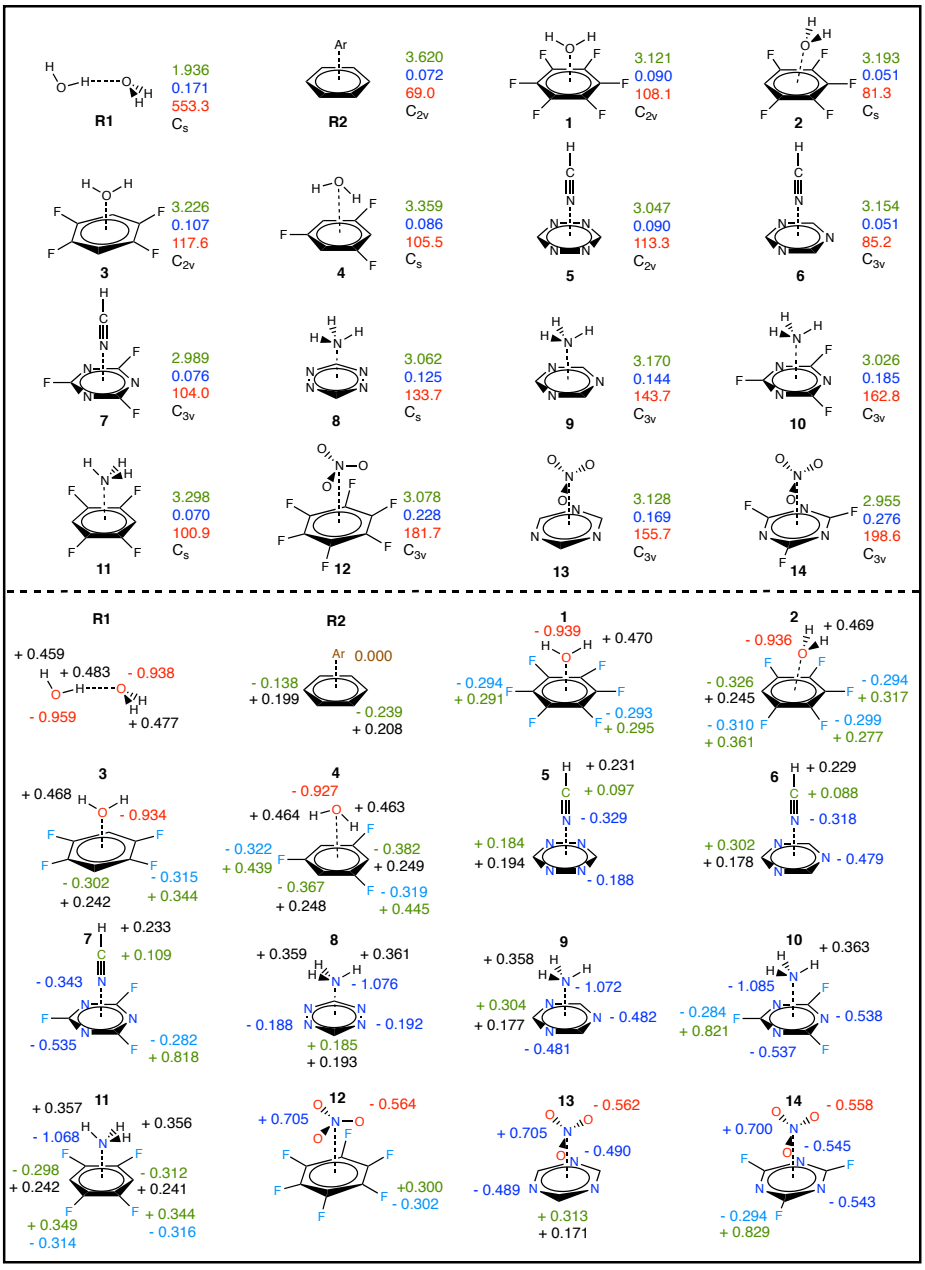


**Figure 3.** Schematics for **R1**, **R2**, and **1–14**, showing: (**top**) molecular geometries, distances $r$ given in green font with units of Å, local vibrational mode LVM force constants $k^a$ (blue font) given in mdyn/Å, corresponding LVM frequencies $\omega^a$ (red) given in $cm^{-1}$, point group (shown in black); and (**bottom**) selected NBO charges: C–atomic charges given in green, O–atomic charges in red, N–atomic charges in blue, F–atomic charges in light blue, and H–atomic charges are shown in black. NBO charges are given in A.U.

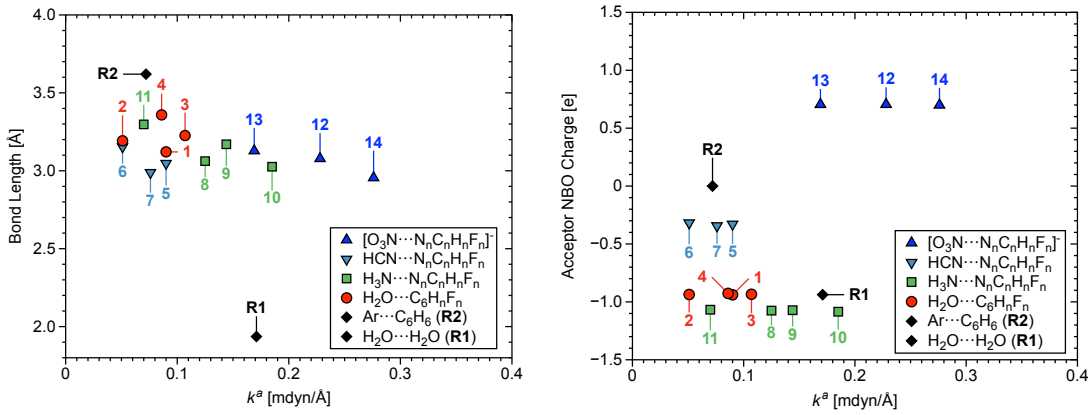


(**a**) (**b**)

**Figure 4.** Calculated at the $\omega$B97X–D/aug–cc–pVTZ level of theory, (**a**) $r$, and (**b**) NBO charges of the central acceptor atoms O and N; plotted with respect to $k^a$ of $\pi$–hole interactions in **1–14**.

There is weak correlation at best between $r$ and $k^a$, which becomes weaker by presence of **R1** and **R2**. The $\pi$–hole interaction length in **14** is 1.000 Å longer than the HB in **R1**, yet the former has a $k^a$ value 0.100 mdyn/Å larger than the latter. The Ar···$C_6H_6$ interaction in **R2** is at least 0.200 Å longer than all 14 $\pi$–hole interactions, but is stronger than **2**, **6**, and **11**. Figure 5a,b show charge transfer (CT) and BE counterpoise corrected for basis set superposition error; both plotted with respect to $k^a$. CT was calculated as the transfer of charge between the acceptor lp–donor atom and the aryl ring. Both of these parameters correlate weakly with bond strength in terms of $k^a$, but BE and $k^a$ show the best correlation of any properties considered in this work. Increase in magnitude of BE weakly correlates with increase in bond strength. The HB in **R1** has a $k^a$ value three times larger than the weakest $\pi$–hole interactions (**2** and **6**). On the other hand, **14** contains the strongest $\pi$–hole interaction in this work with a $k^a$ value 60% larger than $k^a$ of the HB in **R1**.

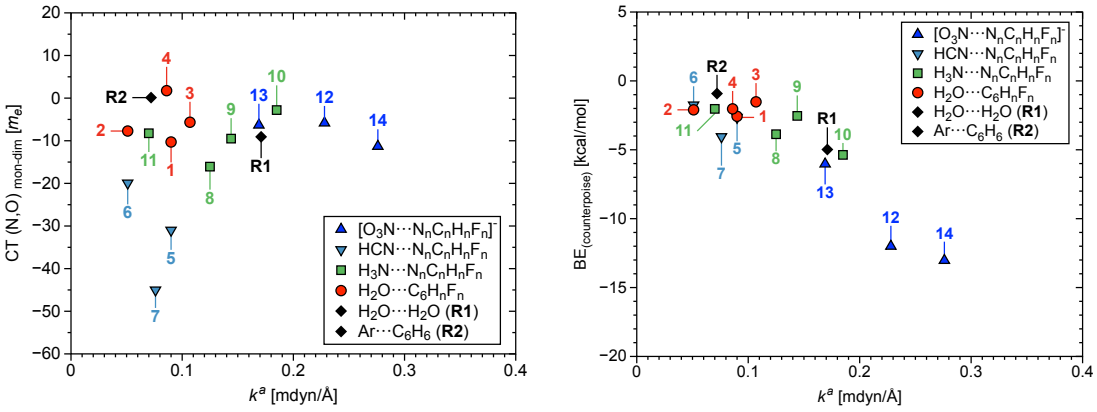


(**a**) (**b**)

**Figure 5.** (**a**) CT (from central $\pi$–hole acceptor atom O in **1–4**, N in **5–14**, Ar in **R2**, and HB acceptor atom O in **R1** $\longrightarrow$ donor), and (**b**) BE, counterpoise corrected for basis set superposition error; both plotted with respect to $k^a$ of $\pi$–hole interactions in **1–14.**

In Figure 6a, the Laplacian of the electron density ($\nabla^2\rho(\mathbf{r}_{CCP})$), where CCP is a cage critical point encompassing N– or O–atoms from the acceptor and aryl C or N–atoms from the donor, is plotted with respect to $k^a$. $\nabla^2\rho(\mathbf{r}_{CCP})$ tracks regions of local charge concentration/depletion [134]. $\nabla^2\rho(\mathbf{r}_{CCP})$ increases with increasing strength of the $\pi$–hole interaction. In other words, increased local concentration of charge at the CCP corresponds to a stronger $\pi$–hole interaction. Figure 6b shows

correlation between $r$ of the HBs and their $k^a$ values, where increased bond length corresponds to weakening of the HB. Figure 7 shows combined $k^a$ values of all SBIs/HBs per $\pi$–hole system, plotted with respect to $k^a$ of the $\pi$–hole interaction; where the larger quantity of stronger SBIs/HBs weakly correlate with stronger $\pi$–hole interactions. This correlation is weak because the HB can strengthen or weaken the $\pi$–hole, depending on the directionality of HB donation; a topic which is discussed further in Section 3.5.

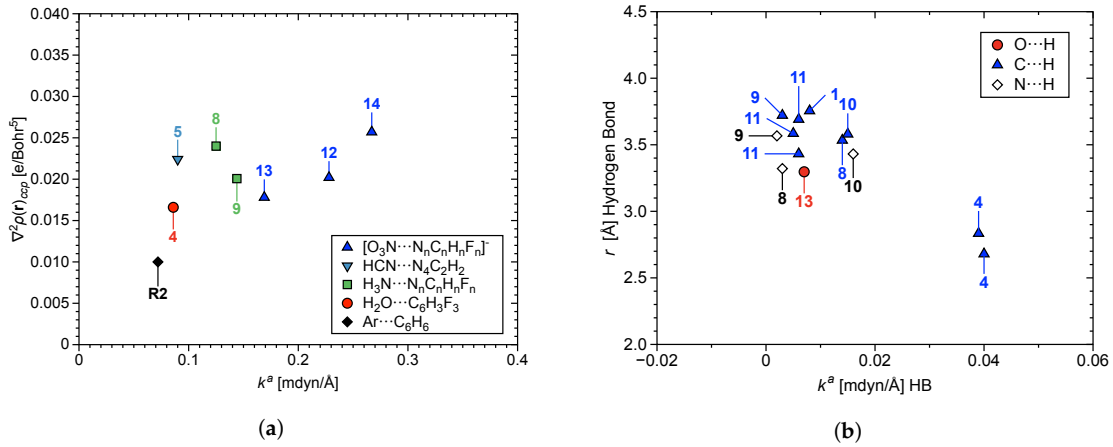


(**a**) (**b**)

**Figure 6.** (**a**) The Laplacian of the electron density at the CCP ($\nabla^2\rho(\mathbf{r}_{CCP})$), and (**b**) $r$ of the HBs; both plotted with respect to $k^a$ of $\pi$–hole interactions in **1–14** and **R2**.

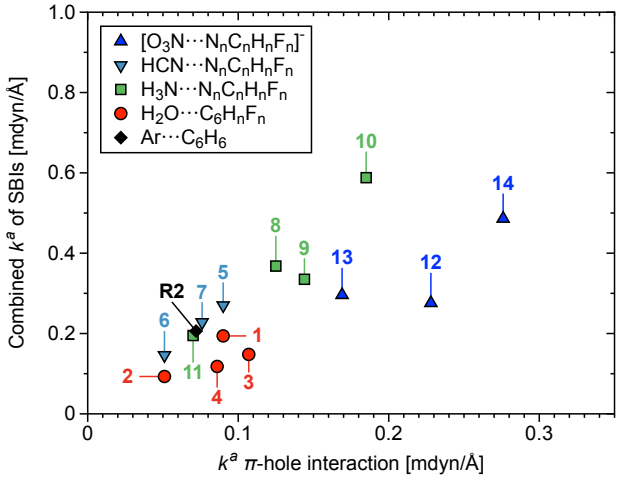


**Figure 7.** Combined $k^a$ values of all SBIs (including HBs) plotted with respect to $k^a$ of $\pi$–hole interactions in **1–14** and **R2**.

Table 4 summarizes LVM data for all HBs between donor/acceptor pairs. Figure 8 is a schematic of the atom labelling/numbering convention used in subsequent tables and figures. HBs were not found in systems **2–3, 5–7, 12,** and **14**. In **2**, the aryl C–atom bound to the lone H–substituent has a charge of −0.326 e, but the orientation of the water molecule eliminates the possibility of HB. The other five aryl C–atoms all carry positive charges with values between +0.277 e and +0.361 e. A bonding interaction between positive charges on aryl C–atoms and positive charges on acceptor H–atoms (+0.469 e) is not favored. Acceptor H–atoms in **3** do not form HBs because they are oriented such that they are not in plane with any of the aryl atoms or substituents and their distance from aryl C–atoms is maximized at the given conformation. It was expected that **5–7**, **12**, and **14** would not form HBs for obvious reasons. Interestingly, **13** is the only example of HB between acceptor and aryl-substituents, where the three $\pi$–hole acceptor nitro O–atoms interact weakly with the three aryl H–atoms.

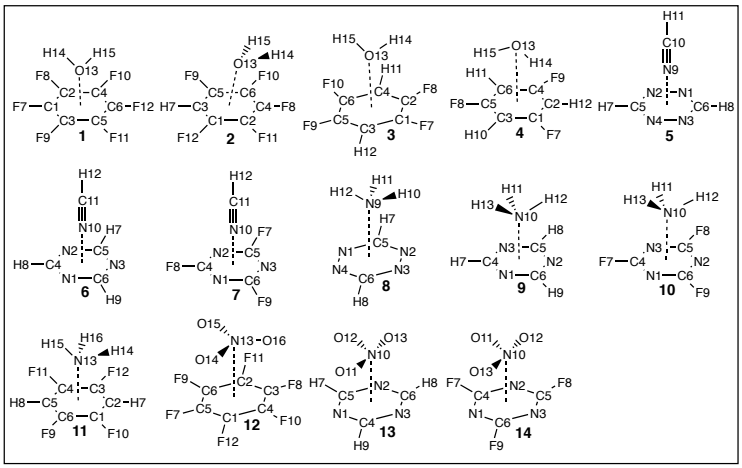

**Figure 8.** Schematic showing all atom numbers in **1–14**, for use as a reference to Tables 4 and 5.

**Table 4.** LVM analysis: $r$, $k^a$, and $\omega^a$, for secondary bonding interactions SBI involving hydrogen atoms in **1, 4, 8–11,** and **13**.

| # | Parameter | $r$ | $k^a$ | $\omega^a$ | Parameter | $r$ | $k^a$ | $\omega^a$ |
|---|---|---|---|---|---|---|---|---|
| **1** | H14···C1 | 3.755 | 0.008 | 124.2 | H15···C6 | 3.755 | 0.008 | 124.2 |
| **4** | H14···C1 | 2.834 | 0.039 | 267.5 | H14···C4 | 2.834 | 0.039 | 267.5 |
| | H14···C2 | 2.680 | 0.040 | 270.1 | - | - | - | - |
| **8** | H10···C6 | 3.534 | 0.014 | 159.8 | H11···N4 | 3.321 | 0.003 | 76.0 |
| | H11···N1 | 3.321 | 0.003 | 76.0 | H12···C5 | 3.534 | 0.014 | 159.8 |
| **9** | H11···N3 | 3.567 | 0.002 | 60.6 | H12···C6 | 3.721 | 0.003 | 72.8 |
| | H11···C4 | 3.721 | 0.003 | 71.1 | H13···N1 | 3.567 | 0.002 | 61.7 |
| | H11···C5 | 3.721 | 0.003 | 70.4 | H13···C4 | 3.721 | 0.003 | 72.3 |
| | H12···N2 | 3.567 | 0.002 | 63.0 | H13···C6 | 3.721 | 0.003 | 71.1 |
| | H12···C5 | 3.721 | 0.003 | 73.3 | - | - | - | - |
| **10** | H11···N3 | 3.431 | 0.016 | 169.2 | H12···C6 | 3.580 | 0.015 | 163.3 |
| | H11···C4 | 3.580 | 0.015 | 163.2 | H13···N1 | 3.431 | 0.016 | 169.2 |
| | H11···C5 | 3.580 | 0.015 | 163.3 | H13···C4 | 3.580 | 0.015 | 163.1 |
| | H12···N2 | 3.431 | 0.016 | 169.3 | H13···C6 | 3.580 | 0.015 | 163.3 |
| | H12···C5 | 3.580 | 0.015 | 163.1 | - | - | - | - |
| **11** | H14···C1 | 3.432 | 0.006 | 108.4 | H16···C2 | 3.585 | 0.005 | 91.9 |
| | H14···C2 | 3.585 | 0.005 | 91.9 | H16···C3 | 3.432 | 0.006 | 108.4 |
| | H14···C6 | 3.691 | 0.005 | 91.0 | H16···C4 | 3.691 | 0.005 | 91.0 |
| **13** | O11···H9 | 3.297 | 0.007 | 108.8 | O13···H8 | 3.297 | 0.007 | 108.6 |
| | O12···H7 | 3.297 | 0.007 | 108.3 | - | - | - | - |

Units for LVM data are given as follows: $r$ in Å, $k^a$ in mdyn/Å, and $\omega^a$ in $cm^{-1}$.

Table 5 summarizes LVM data for all SBIs found in **1–14**, excluding HBs; where 13 of the 14 $\pi$–hole systems contains at as few as six non–HB SBIs (systems **1–3**, **5–11**, and **14**), 12 non-HB SBIs (**12**), and as many as 15 (system **13**) non–HB SBIs of the following type: C···O, C···N, or N···N; where the first atom listed (C/N) is from the $\pi$–hole donor and the second atom (O/N) is from the acceptor (donor···acceptor). In most cases, there is a LVM between the $\pi$–hole acceptor and all six atoms of the aryl ring; with **4** being the exception. The remainder of this section is divided into four subsections pertaining to significant factors for modulation of molecular geometry, bond strength, and the intrinsic nature of the $\pi$–hole interactions: *(3.3) Aryl Substituent Effects, (3.4) Nature of the Aryl Rings, (3.5) Secondary Bonding Interactions and (3.6) Characterization of Normal Vibrational Modes.*

**Table 5.** Summary of LVM data: $r$, $k^a$, and $\omega^a$ for secondary bonding interactions SBI not including hydrogen atoms, for **1–14**.

| # | Parameter | $r$ | $k^a$ | $\omega^a$ | Parameter | $r$ | $k^a$ | $\omega^a$ |
|---|---|---|---|---|---|---|---|---|
| **R2** | Ar13···C1 | 3.877 | 0.031 | 76.0 | Ar13···C4 | 3.877 | 0.031 | 76.0 |
| | Ar13···C2 | 3.877 | 0.036 | 80.8 | Ar13···C5 | 3.877 | 0.036 | 80.8 |
| | Ar13···C3 | 3.877 | 0.036 | 80.8 | Ar13···C6 | 3.877 | 0.036 | 80.8 |
| **1** | O13···C1 | 3.414 | 0.027 | 81.5 | O13···C4 | 3.415 | 0.031 | 87.7 |
| | O13···C2 | 3.415 | 0.031 | 87.7 | O13···C5 | 3.415 | 0.031 | 87.7 |
| | O13···C3 | 3.415 | 0.031 | 87.7 | O13···C6 | 3.414 | 0.027 | 81.5 |
| **2** | O13···C1 | 3.551 | 0.012 | 53.6 | O13···C4 | 3.320 | 0.027 | 81.8 |
| | O13···C2 | 3.402 | 0.015 | 61.2 | O13···C5 | 3.551 | 0.012 | 53.6 |
| | O13···C3 | 3.637 | 0.012 | 54.7 | O13···C6 | 3.402 | 0.015 | 61.2 |
| **3** | O13···C1 | 3.515 | 0.022 | 74.4 | O13···C4 | 3.515 | 0.022 | 74.4 |
| . | O13···C2 | 3.506 | 0.026 | 80.1 | O13···C5 | 3.506 | 0.026 | 80.1 |
| | O13···C3 | 3.506 | 0.026 | 80.1 | O13···C6 | 3.506 | 0.026 | 80.1 |
| **5** | N9···C1 | 3.342 | 0.044 | 102.9 | N9···C4 | 3.342 | 0.044 | 102.9 |
| | N9···C2 | 3.342 | 0.044 | 102.9 | N9···C5 | 3.279 | 0.047 | 111.6 |
| | N9···C3 | 3.342 | 0.044 | 102.9 | N9···C6 | 3.279 | 0.047 | 111.6 |
| **6** | N10···N1 | 3.437 | 0.024 | 75.9 | N10···C4 | 3.405 | 0.025 | 80.6 |
| | N10···N2 | 3.437 | 0.024 | 75.8 | N10···C5 | 3.405 | 0.025 | 80.5 |
| | N10···N3 | 3.437 | 0.024 | 76.6 | N10···C6 | 3.405 | 0.024 | 80.2 |
| **7** | N10···N1 | 3.288 | 0.038 | 95.8 | N10···C4 | 3.240 | 0.038 | 100.1 |
| | N10···N2 | 3.288 | 0.038 | 95.7 | N10···C5 | 3.240 | 0.038 | 100.0 |
| | N10···N3 | 3.288 | 0.038 | 95.7 | N10···C6 | 3.240 | 0.038 | 100.1 |
| **8** | N9···N1 | 3.316 | 0.059 | 119.5 | N9···N4 | 3.316 | 0.059 | 119.5 |
| | N9···N2 | 3.398 | 0.045 | 104.0 | N9···C5 | 3.290 | 0.063 | 128.1 |
| | N9···N3 | 3.398 | 0.045 | 104.0 | N9···C6 | 3.290 | 0.063 | 128.1 |
| **9** | N10···N1 | 3.452 | 0.049 | 108.5 | N10···C4 | 3.419 | 0.056 | 121.2 |
| | N10···N2 | 3.452 | 0.049 | 109.1 | N10···C5 | 3.419 | 0.055 | 120.2 |
| | N10···N3 | 3.452 | 0.048 | 108.0 | N10···C6 | 3.419 | 0.054 | 119.4 |
| **10** | N10···N1 | 3.222 | 0.074 | 133.8 | N10···C4 | 3.273 | 0.076 | 140.9 |
| | N10···N2 | 3.222 | 0.074 | 133.9 | N10···C5 | 3.273 | 0.076 | 140.9 |
| | N10···N3 | 3.222 | 0.074 | 133.8 | N10···C6 | 3.273 | 0.076 | 140.9 |
| **11** | N13···C1 | 3.557 | 0.021 | 74.6 | N13···C4 | 3.587 | 0.022 | 76.3 |
| | N13···C2 | 3.552 | 0.036 | 97.3 | N13···C5 | 3.611 | 0.041 | 103.7 |
| | N13···C3 | 3.557 | 0.021 | 74.6 | N13···C6 | 3.587 | 0.022 | 76.3 |
| **12** | N13···C1 | 3.375 | 0.031 | 90.6 | O14···C1 | 3.149 | 0.015 | 61.2 |
| | N13···C2 | 3.375 | 0.031 | 90.6 | O14···C5 | 3.149 | 0.015 | 61.2 |
| | N13···C3 | 3.375 | 0.031 | 90.6 | O15···C2 | 3.149 | 0.015 | 61.2 |
| | N13···C4 | 3.375 | 0.031 | 90.6 | O15···C6 | 3.149 | 0.015 | 61.2 |
| | N13···C5 | 3.375 | 0.031 | 90.6 | O16···C3 | 3.149 | 0.015 | 61.2 |
| | N13···C6 | 3.375 | 0.031 | 90.6 | O16···C4 | 3.149 | 0.015 | 61.2 |
| **13** | N10···N1 | 3.419 | 0.022 | 72.3 | O11···C4 | 3.117 | 0.017 | 64.1 |
| | N10···N2 | 3.419 | 0.022 | 72.4 | O12···N1 | 3.394 | 0.016 | 59.7 |
| | N10···N3 | 3.419 | 0.021 | 72.0 | O12···N2 | 3.394 | 0.016 | 59.7 |
| | N10···C4 | 3.375 | 0.021 | 73.8 | O12···C5 | 3.117 | 0.017 | 64.0 |
| | N10···C5 | 3.375 | 0.021 | 73.5 | O13···N2 | 3.394 | 0.016 | 59.6 |
| | N10···C6 | 3.375 | 0.021 | 73.7 | O13···N3 | 3.394 | 0.016 | 59.5 |
| | O11···N1 | 3.394 | 0.016 | 59.6 | O13···C6 | 3.117 | 0.017 | 64.1 |
| | O11···N3 | 3.394 | 0.016 | 59.4 | - | - | - | - |
| **14** | N10···C4 | 3.205 | 0.134 | 187.7 | O11···C4 | 2.936 | 0.028 | 83.6 |
| | N10···C5 | 3.205 | 0.134 | 187.7 | O11···C5 | 2.936 | 0.028 | 83.6 |
| | N10···C6 | 3.205 | 0.134 | 187.7 | O11···C6 | 2.936 | 0.028 | 83.6 |

Units for computational data are given as follows: $r$ in Å, $k^a$ in mdyn/Å, and $\omega^a$ in $cm^{-1}$.

### *3.3. Aryl Substituent Effects*

Systems **1–4** are a good starting point to systematically analyze substituent effects. The donor in **1** is $C_6F_6$, the donor in **2** is $C_6F_5H$, $C_6F_4H_2$ in **3**, and $C_6F_3H_3$ in **4**. One effect is the physical response of acceptor to decreasing the number of aryl F-substituents. Each of the four water molecules in **1–4** is oriented quite differently from one another with respect to the aryl ring. **1** has $C_{2v}$ symmetry, with the acceptor H–atoms pointing opposite the aryl ring. Each atom of the water molecule rests in plane with two aryl C−F groups positioned para to each other. Unexpectedly, the $\pi$–hole interaction in **1** is not particularly strong ($k^a = 0.090$ mdyn/Å) compared to the rest of $H_2O$ acceptor group **2–4**, systems **5–14**, and even **R1** and **R2**. The six aryl F–substituents induce a sizable $\pi$–hole with large positive ESP which therefore should promote stronger $\pi$–hole interactions, but this effect is countered by a lack of cooperation between atoms of the aryl donor and atoms of the $H_2O$ acceptor in forming SBIs [135]. Furthermore, there are two weak C···H donor/acceptor SBIs ($k^a = 0.008$ mdyn/Å) in **1** (see Table 4).

Compared to **1**, the acceptor H–atoms in **2** are rotated nearly 90° to avoid repulsive forces from the donor H–atom. The aryl C–atom bound to H has a negative charge of −0.326 e; whereas the aryl–C atom para to the lone C−H bond has a charge of +0.317 e. In contrast, all C–atoms in **1** have positive charges (see Figures 3 and 8) of +0.295 e (C2 through C5) and +0.291 e (C1 and C6). The negative charge on the C–atom in **2** repels the electron rich acceptor O–atom toward the opposite end of the ring, resulting in the $\pi$–hole interaction distance increasing 0.072 Å compared to **1**. The O–atom is also no longer directly over the $\pi$–hole, which decreases orbital overlap. Instead, the O–atom is 0.407 Å closer to the C–atom para to C−H. Furthermore, the $\pi$–hole should migrate closer to the C−F group, and become weaker its ESP becomes more negative. The cumulative effect is that substitution of a single aryl F–atom for H disrupts the molecular symmetry, hinders the reactivity of the $\pi$–hole, and decreases $k^a$ of the $\pi$–hole interaction in **2** by nearly 50% compared to **1**; the $\pi$–hole interaction in **2** is the weakest of the $H_2O$ acceptor systems **1–4**. Although system **2** is an extreme case, where the other aryl rings of **1, 3–4** are significantly more symmetric, there is clear indication that substituent effects involving the aryl ring can significantly weaken/strengthen the $\pi$–hole interaction and drastically alter the molecular geometry of the system. The strongest $\pi$–hole interaction among systems **1–4** occurs in **3**, which has $C_{2v}$ symmetry with acceptor H–atoms still oriented away from the aryl ring. The water molecule forms a plane perpendicular to the two FC=CF bonds of the donor. The water O−H bonds in **3** ($k^a = 8.549$ mdyn/Å), are stronger than the O−H bonds in **1, 2**, and **4** (between 8.532 and 8.547 mdyn/Å). This increase in O−H bond strength has a net stabilizing effect on the whole system, which extends to the $\pi$–hole interaction. The orientations of $H_2O$ and the aryl F–substituents also benefit the $\pi$–hole interaction in system **3**; as any possible repulsive forces between the donor/accepter occur over maximum distances compared to **1, 2,** and **4**, and the position of the $\pi$–hole is not affected due to the symmetry of the $C_6F_4H_2$ ring.

**4** has 3 aryl F–substituents and 3 H–substituents, arranged symmetrically in an alternating pattern. Addition of the third H–substituent resulted in inversion of the acceptor H–atoms, which now point toward the aryl ring. $H_2O$ is coplanar with para aryl C−H and C−F groups (C2−H12 and C5−F8). The acceptor atom H14 points downward toward C2, which is caused by the charge of −0.382 e on C2. The opposite occurs between acceptor–H15/donor–C5, where positive charges on each atom are repulsive. The H15···C5 distance is 0.388 Å longer than H14···C2 as a result. The $\pi$–hole interaction in **4** is only slightly weaker than **1** (by 0.004 mdyn/Å), an unexpected result based on substituent effects alone; as the O acceptor in **1** should interact much more strongly with its $\pi$–hole. However, other factors must be considered. The acceptor H14 in **4** can HB with the negatively charged C2 donor atom, yet is in close enough proximity to bind to C4. A third HB was found in **4**; all three HBs are of the C···H−O type, and are among the strongest HBs in systems **1–14** (see Table 4). This factor is discussed with more detail in Section 3.5. Perhaps the most surprising substituent effect (or lack there of) is an absence of intermolecular interactions involving aryl–substituents and the $\pi$–hole acceptors. There is only one such SBI; it is in system **13** and is a O···H−C type HB. This interaction is discussed further in Section 3.5.

### *3.4. Nature of the Aryl Rings*

In **5–7**, the influence of SBIs is minimized, and each aryl ring contains four, three, and three N–atoms, respectively. **5** has $C_{2v}$ symmetry while **6** and **7** have $C_{3v}$ symmetry. N–substitution, atomic nature of the aryl ring, and three-fold symmetric F–substitution do not cause significant symmetry related changes in this case. However, it turns out that **5–7** have the weakest $\pi$–hole interaction strength on average compared to the $H_2O$ acceptor (**1–4**), $NH_3$ acceptor (**8–11**), and $NO_3^-$ acceptor (**12–14**) $\pi$–hole systems. One key difference between systems **5–7** and the systems just mentioned is the orientation and nature of the HCN acceptor in **5–7**, where the N–atom points downward toward the $\pi$–hole and the H–atom points in the opposite direction. This eliminates the possibility HB donation and decreases the overall possibility of SBIs. System **6** has one less aryl N–atom compared to **5**. The $\pi$–hole interaction in **5** is 0.107 Å shorter and has a $k^a$ value nearly two times larger than the $\pi$–hole interaction in **6**. Incorporating N–atoms into the aryl ring appears to influence strength of the $\pi$–hole interaction more than F–substitution. The difference between donors of **6** and **7**, is a three fold F–substitution in the latter, which increases strength of the $\pi$–hole interaction by 0.024 mdyn/Å. Though significant, triple F–substitution is not able to modulate strength of the $\pi$–hole interaction as much as insertion/removal of aryl donor N–atoms, as is the case for **5** and **6**. Integration of a fourth N–atom to the aryl ring nearly doubles $k^a$ of the interaction; whereas substituting three C−H groups for three C−F groups achieves an increase in interaction strength by approximately 50%. The NBO picture suggests the $N_4C_2H_2$ donor of **5** supports a more delocalized electronic density compared with the $N_3C_3H_3$ donor in **6** and $N_3C_3F_3$ in **7**. There is a CT of −30.99 milli-electrons ($m_e$) from the acceptor N–atom to the aryl ring in **5**, approximately –10 $m_e$ more than in **6** but roughly −15 $m_e$ less than CT in **7**. In addition to being the weakest interactions and not participating in HB, **5–7** also have the three largest CT values among **1–14**. Correlation between CT and $k^a$ for **1–14** is very weak, but the general trend is that the $\pi$–hole interactions are stronger when CT gets closer to zero (see Figure 5a).

**8–14** are not ideal for investigating how the nature of the aryl ring influences the $\pi$–hole interaction, given that the acceptors in these systems are ammonia and the nitrate anion. Each of the three acceptor H–/O–atoms are able to form SBIs, which make it difficult to assess both substituent effects and how addition of N–atoms into the aryl ring can influence the $\pi$–hole interaction. This is also evident in the case of **1–7**, where the acceptors each have one less atom than the acceptors in **8–14**. On the other hand, this makes **8–14** ideal for studying the effect of SBIs on $\pi$–hole interactions.

### *3.5. Secondary Bonding Interactions*

Of all systems **1–14**, **4** is the only $\pi$–hole system completely void of SBIs between a non-hydrogen acceptor and non-hydrogen donor. However, the unusual orientation of $H_2O$ in **4** puts H14 in close proximity to the C1−C2−C4 region of the aryl ring (see Figure 1 and Tables 4 and 5); where H14···C1, H14···C2, and H14···C4 lengths are 2.834, 2.680, and 2.834 Å, respectively. H14 interacts with all three aryl C–atoms, and the resultant HBs are among the strongest found in **1–14**. The effect of these HBs is stabilization and increased strength of the $\pi$–hole interaction by 0.035 mdyn/Å compared to system **2**, where the acceptor O–atom forms SBIs with the donor aryl C–atoms. **2** and **3** do not have any HBs, but all of their aryl C–atoms interact with the acceptor O–atom. **2** has the weakest $\pi$–hole interaction of **1–14**, which is largely due to the nature of the donor and the arrangement of the acceptor water molecule, but a contributing effect is that five of the six C···O interactions are among the weakest for **1–14** (see Table 5). The HBs in system **1**, are nearly the weakest (0.008 mdyn/Å) interactions found in **1–14**. Although these HBs do stabilize and increase strength of the $\pi$–hole interaction, stronger HBs will promote stronger $\pi$–hole interactions [136]. For example, system **4** contains the same type of C···H HB found in system **1**, but the $k^a$ values of HBs in the former are 5 times larger than in the latter. Also, system **4** has three HBs while system **1** has two. The $\pi$–hole in **1** should be larger and have more positive ESP compared to **4**, due to the nature of the aryl substituents (six F–atoms in **1**, three F– and three H–atoms in **4**). In addition, the lp is more accessible in **1**, compared to **4** where the H–atoms point toward the aryl ring. Also, O13 is 0.238 Å closer to the $\pi$–hole in system **1**. Despite all of these

factors, $k^a$ of the $\pi$–hole interaction in **4** is within 0.004 mdyn/Å of the $\pi$–hole interaction in **1**. This a result of the comparatively strong HBs in system **4** providing stability and increasing strength of the $\pi$–hole interaction.

Although **5–7** do not provide information on the effect HBs have on the $\pi$–hole interaction, a clear picture emerges in terms of the role other SBIs play. In terms of strength of the $\pi$–hole interaction, the sequence is: **5** > **7** > **6**. This matches the trend in $k^a$ of the N···N and C···N donor/acceptor SBIs. For C···N in **5**, $k^a = 0.044$ and 0.047 mdyn/Å, for N···N and C···N in **6**, $k^a = 0.024$ and 0.025 mdyn/Å, and for N···N/C···N in **7**, $k^a = 0.038$ mdyn/Å. This indicates that non-HB SBIs may play a cooperative role, where they help to strengthen $\pi$–hole interactions. However, HBs seem to have a more significant effect on the $\pi$–hole interaction comparatively.

**8–11** are the only $\pi$–hole acceptors where each system participates in HB and SBIs between aryl C or N atoms and the central acceptor N–atom. In terms of $\pi$–hole interaction strength, the sequence is: **10** > **9** > **8** > **11**. The $\pi$–hole interaction in **8** should be stronger than **9** based on the nature of the aryl donor, but the ammonia H–atoms in **8** are staggered such that they are centered above the bonds encompassing the ring. H12 is oriented above an N–N bond, and the other two ammonia H–atoms orient above two of the aromatic C–N bonds. This results in **8** having fewer HBs compared to **9–11**. The N···N and C···N donor/acceptor interactions in **8** are slightly shorter and slightly stronger than comparable interactions in **9**. The same type of inter–monomer N···N and C···N interactions in system **10** are the strongest amongst the $NH_3$–acceptor group by at least 0.026 mdyn/Å for N···N and at least 0.055 mdyn/Å for C···N. Strength of the non–HB SBIs trends similarly to the $\pi$–hole interaction strength order: **10** > **9** ≈ **8** > **11**. This not the case with individual HB strength. However, when HB strength is considered as a sum of each individual HB per $\pi$–hole system, the collective HB strength matches the trend of $\pi$–hole interaction strength. HBs are effecting the system compared to the non-HB SBIs. **11** has the weakest $\pi$–hole interaction, the weakest collective HB strength, the weakest non–HB SBIs, the fewest N–aromatic atoms (zero), and the most F–substituents of **8–11**. Although SBIs are predominant in **8–11**, it turns out that N–aromatic atoms still play a major role in modulating bond strength; with N–aromatic systems having $\pi$–hole interaction $k^a$ values increase 100% compared to the species with a $C_6$ ring. Though even less significant than the aforementioned, effects of F–substitution are again apparent when comparing systems **9** and **10**; where the F–substituents result in a 28% increase in $k^a$ values.

**12–14** are the only anion $\pi$–hole systems investigated in this work, and as expected, occupy the strong end of $\pi$–hole interaction spectrum. In **12**, $NO_3^-$ has a staggered conformation with respect to the $C_6F_6$ ring which puts the three acceptor O–atoms are at maximal distances from all C and F donor–atoms. Of course, there is no possibility of HBs in **12**, but the negatively charged O–atoms interact with the positively charged aryl C–atoms. The acceptor N–atom also interacts with the aryl C–atoms. This is possible because N has a lone pair and $NO_3^-$ has an excess of delocalized electrons. The $\pi$–hole interaction in **13** is substantially weaker than the interactions in **12** and **14**. Regardless, **12–14** have the three strongest $\pi$–hole interactions among **1–14**, while they have the weakest and fewest number of HBs among each acceptor group. All three acceptor O–atoms in **13** HB with the three H–substituents on the aryl ring. These are the only three HBs where the $\pi$–hole acceptor is also the HB acceptor. In every other case, the directionality of acceptor/donor in the HB is the reverse direction of the $\pi$–hole interaction. Because the HB donor in **13** is the aryl C−H, electronic density is transferred to the aryl ring and throughout the $\pi$–system [137]. This transfer will cause an increase in negative ESP at the $\pi$–hole, which in turn weakens the $\pi$–hole interaction. When the HB donor/acceptor roles are reversed, electronic density transfers from the aryl ring to the acceptor molecule. The depletion of electronic density from the aryl ring increases the positive ESP at the $\pi$–hole, and since the acceptor molecule now has more electronic density, it becomes a better electron donor. When the aryl ring is the HB acceptor, charge on the atoms involved will increase in the positive direction and negative charge is leaving the $\pi$–system. This explains why each HB except for the O···H−C interactions in

**13** help increase the strength of the $\pi$–hole interaction; whereas **13** has a substantially weaker $\pi$–hole interaction compared to **12** and **14** which do not have any HBs.

### *3.6. Characterization of Normal Modes*

In addition to providing $k^a$ and $\omega^a$ and related local vibrational mode properties [80], the local mode analysis has led to a new way of analyzing vibrational spectra. The characterization of normal modes (CNM) procedure decomposes each normal vibrational mode into local mode contributions for a non-redundant set of LVMs by calculating the overlap between each local mode vector with this normal mode vector [77–79,82]. In this way, the character of each normal mode can be uniquely assessed [68,80,138]. In this work we performed a CNM decomposition for **R2** and **1** comparing in particular the contribution of the local vibrational $\pi$–hole-interaction mode to the lower frequency normal modes in both complexes. The corresponding decomposition plots are shown in Figures 9 and 10.

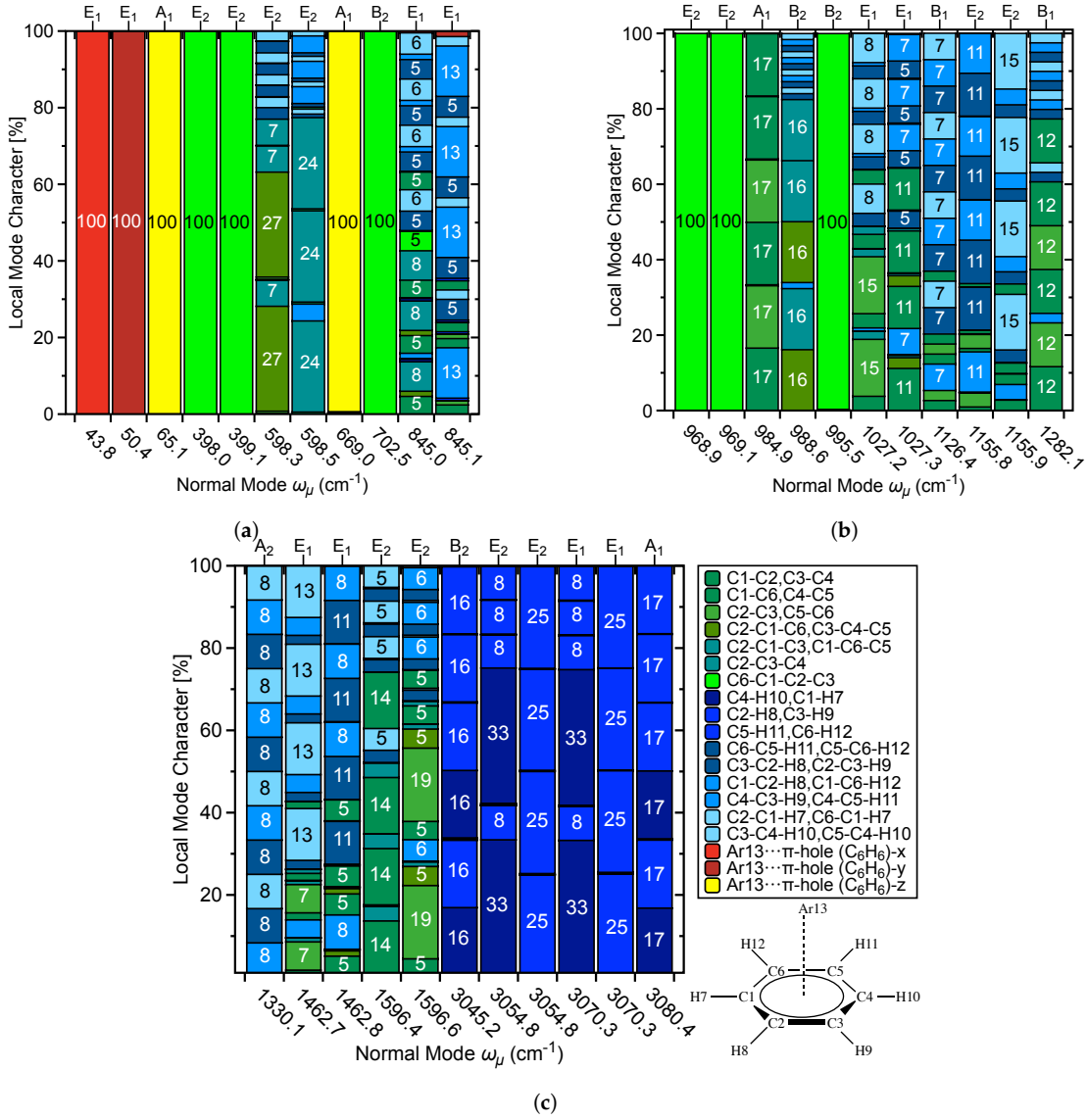


**Figure 9.** Decomposition of normal vibrational modes into % LVM contributions for the Ar···$C_6H_6$ dimer **R2**; (**a**) % LVM contributions to normal vibrational modes 1–11, (**b**) % LVM contributions to normal vibrational modes 12–22, and (**c**) % LVM contributions to normal vibrational modes 23–33.

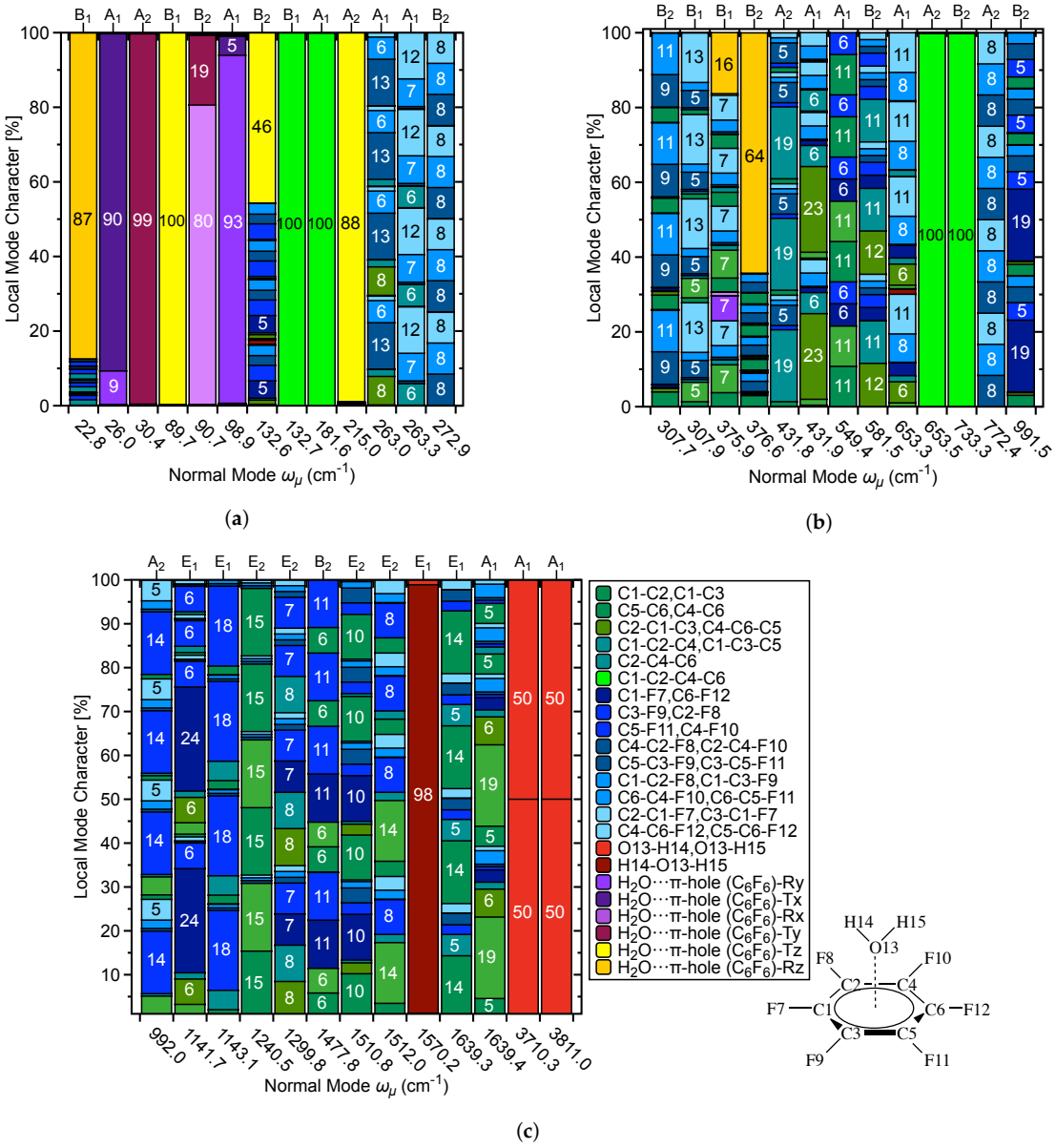


**Figure 10.** Decomposition of normal vibrational modes into % LVM contributions for the $H_2O\cdots C_6F_6$ $\pi$–hole system **1**; (**a**) % LVM contributions to normal vibrational modes 1–13, (**b**) % LVM contributions to normal vibrational modes 14–26, and (**c**) % LVM contributions to normal vibrational modes 27–39.

The set of local modes used for this purpose was chosen to include all inter-monomer local modes. As shown in Figure S1 of the Supplementary Materials there are 9 possible inter-monomer modes, 3 stretching motions (x, y, z direction), 3 rotations (x, y, z direction), and 3 anti-rotations (x, y, z direction). 6 of them are needed to define the set of inter-monomer modes. We generally use the 3 stretching motions labelled $T_x$, $T_y$, and $T_z$ an d 3 rotations $R_x$, $R_y$, $R_z$ in the following. **R2** is a special case with one monomer being an atom reducing the number of inter-monomer modes to 3 translational modes (labelled as x, y, z).

### 3.6.1. Normal Modes Related to the $\pi$–Hole Interaction

In Figure 9a–c, normal modes $\omega_\mu$ are decomposed into % LVM contributions for complex **R2**, and the corresponding CNM plots for complex **1** are given in Figure 10a–c. Figure 9a shows CNM

for $\omega_\mu$ 1–11 ($\omega_{\mu1}$ through $\omega_{\mu11}$) into % LVM contributions for **R2**, where 'x,' 'y,' and 'z' in the Figure legends denote translations of the Ar–atom in the x–, y–, and z–directions with respect to the benzene molecule, as described above. In standard orientation, the Ar$\cdots\pi$–hole interaction is in the z–direction. Correspondingly, the z–component of the three inter-monomer Ar$\cdots\pi$–hole LVM parameters represents the direct Ar$\cdots\pi$–hole interaction, i.e., this is the mode which corresponds to the special force constant $k^a$. It is shown in yellow color in the CMN plots in Figure 10a–c for quick reference.

For **R2**, $\omega_{\mu1}$ through $\omega_{\mu3}$ and $\omega_{\mu8}$ are all 100% LVM character corresponding to inter-monomer vibrations, where $\omega_{\mu3}$ at 65.1 cm$^{-1}$ and $\omega_{\mu8}$ at 669.0 cm$^{-1}$ are dominated by the $\pi$–hole interaction in the z–direction, representing the stretching and contraction the argon atom with regard to the center of the benzene ring. $\omega_{\mu3}$ is characterized by the translational motion of the Ar–atom perpendicular to the plane of the benzene ring, and $\omega_{\mu8}$ represents wagging of the six benzene H–atoms towards and away from the Ar–atom. This mode also perturbs slightly the benzene C–atoms. Movies of the $\omega_{\mu3}$ and $\omega_{\mu8}$ vibrational modes are shown in the Supplementary Materials, see Table S1 for description. Collectively, it is all of the vibrations associated with $\omega_{\mu3}$ and $\omega_{\mu8}$ which are required to accurately describe the $\pi$–hole interaction. These findings clearly emphasize that the special force constant $k^a$ as defined in this work is meaningful.

System **1** consists of 39 $\omega_\mu$ and 39 LVMs, including six parameters describing the inter-monomer translations $T_x$, $T_y$, and $T_z$ and the inter-monomer rotations $R_x$, $R_y$, $R_z$, introduced above, see also legend in Figure 10a–c. As with CNM for **R2**, the direct $\pi$–hole interaction occurs in the z–direction; therefore the z–components of the inter-monomer LVMs are of particular interest and and are represented with a light yellow bar for $T_z$ in Figure 10a,b- and with the darker yellow color for $R_z$.

The z–components of the inter-monomer LVMs contribute to six of the normal modes: $\omega_{\mu1}$ (22.8 cm$^{-1}$), $\omega_{\mu4}$ (89.7 cm$^{-1}$), $\omega_{\mu7}$ (132.6 cm$^{-1}$), $\omega_{\mu10}$ (215.0 cm$^{-1}$), $\omega_{\mu16}$ (375.9 cm$^{-1}$), and $\omega_{\mu17}$ (376.6 cm$^{-1}$). The $R_z$ LVM composes 87% of $\omega_{\mu1}$, with C−F/C−C LVMs accounting for the remaining 13% (Figure 10a). The $R_z$ component is much less significant for the $\pi$–hole interaction, but mixing of C–C, C–F, and $R_z$ contributions to $\omega_{\mu1}$ imply this mode likely relates more to the HBs found in **1**. The motion of $\omega_{\mu1}$ involves rotation of acceptor H–atoms about the O–atom, parallel to the plane of the donor ring. Description of $\omega_{\mu4}$ in **1** is comparable to $\omega_{\mu3}$ of **R2**, which is translation of the acceptor molecule in the z–direction. This normal mode is of 100% $T_z$ character. Therefore, it could be used in experimental spectra as quick identification of the $\pi$–hole interaction. The motion of the water molecule in $\omega_{\mu4}$ perturbs the $C_6F_6$ slightly; whereas this does not occur in **R2**. The frequency of the former is also larger than the latter by 24.6 cm$^{-1}$.

The $\omega_{\mu7}$ contains 46 % $T_z$ character combined with small contributions from the C–F, C–C–F, and H–O–H LVMs. This mode is comparable to $\omega_{\mu8}$ of **R2**: the z-direction wagging of the aryl substituents. As with the previous comparison, the wagging motion of the aryl–F atoms perturbs the acceptor molecule and the aryl C–atoms in **1**; this not the case for **R2**. On the other hand, similarly to **R2**, this mode is also important for a full description of the $\pi$–hole interaction. $T_z$ accounts for 88% of $\omega_{\mu10}$ and describes the translation of the aryl C–atoms in the z–direction. This mode strongly perturbs the acceptor $H_2O$ molecule, and there is no comparable mode to this in **R2**. The $\omega_{\mu10}$ is also a main component of the $\pi$–hole interaction, as the six aryl C–atoms move in phase and therefore translate the $\pi$–hole directly toward the acceptor. The $\omega_{\mu16}$ and $\omega_{\mu17}$ represent z–rotation of the four equivalent aryl C–atoms and z–rotation of the two equivalent aryl C–atoms, respectively. $R_z$ compose 16% of $\omega_{\mu16}$ and 64% of $\omega_{\mu17}$. These modes do not strongly effect $\pi$–hole interactions. However, $\omega_{\mu17}$ is related to the HBs between acceptor/donor, where the HB acceptor C–atoms rotate in the direction of the water H–atoms. This explains why the contribution from $R_z$ is much larger for $\omega_{\mu17}$. As was previously mentioned, the HBs with directionality opposite to that of the $\pi$–hole interaction effectively stabilize and increase strength of the $\pi$–hole interaction. This relationship is reflected in the CNM analysis. It is evident that the $\pi$–hole interaction in **1** is stronger than in **R2** based on the CNM because the inter-monomer LVMs $T_z$ and $R_z$ of **1** compose more of $\omega_\mu$, the comparable frequencies are larger tahnin **1**, and the vibrational modes are much more strongly coupled between monomers in **1**. Movies

of the $\omega_{\mu 1}$, $\omega_{\mu 4}$, $\omega_{\mu 7}$, $\omega_{\mu 10}$, and $\omega_{\mu 17}$ vibrational modes are shown in the Supplementary Materials, see Table S1 for description.

3.6.2. Normal Modes Not Related to the $\pi$–Hole Interaction

The C6−C1−C2−C3 dihedral mode is the only LVM contributor to $\omega_{\mu 4}$ through $\omega_{\mu 5}$ and $\omega_{\mu 9}$. Modes 6–7 are composed of mainly angular C−C−C contributions with small components of the various C−C−H contributions. Mode 10 at 845.0 $cm^{-1}$ consists of a nearly even mixture of C−C−C and C−C−H LVM contributions with small (5%) contribution from C6−C1−C2−C3; whereas mode 11 is C−C−H dominant with minor C−C−C, and C−H character. Figure 9b shows decomposition of $\omega_{\mu}$ into % LVM contributions for $\omega_{\mu 12}$ through $\omega_{\mu 22}$ in **R2**. Again, the C6−C1−C2−C3 dihedral is the sole contribution to $\omega_{\mu 12}$ through $\omega_{\mu 13}$ and $\omega_{\mu 16}$. The six C−C LVMs compose $\omega_{\mu 14}$ and are the largest components of $\omega_{\mu 18}$ and $\omega_{\mu 22}$, with minor components being the C−C−H LVMs. C−C−C LVMs compose 80% of $\omega_{\mu 15}$ with C−C−H contributions accounting for the remaining 20%. At 1126.4 $cm^{-1}$ through 1155.9 $cm^{-1}$, $\omega_{\mu 19}$ through $\omega_{\mu 21}$ are C−C−H LVM dominant with small contributions. In Figure 9c, the remaining $\omega_{\mu}$ (23–33) are decomposed into % LVM contributions for **R2**. C−C−H LVMs are the major contributions to $\omega_{\mu 23}$ through $\omega_{\mu 25}$: 100% of $\omega_{\mu 23}$ at 1330.1 $cm^{-1}$, nearly 80% of $\omega_{\mu 24}$ at 1462.7 $cm^{-1}$, and 76% of $\omega_{\mu 25}$ at 1462.8 $cm^{-1}$. C−C LVM contributions steadily increase from $\omega_{\mu 24}$ through $\omega_{\mu 27}$ (1462.7 $cm^{-1}$ through 1596.9 $cm^{-1}$), where % LVM contributions increase from 20 % of the former to nearly 70 % of the latter. The six highest $\omega_{\mu}$ (28–33) span 3045.2 $cm^{-1}$ through 3080.4 $cm^{-1}$ and are composed entirely of C−H LVMs.

$\omega_{\mu 7}$ (132.6 $cm^{-1}$) and $\omega_{\mu 11}$ through $\omega_{\mu 15}$ (263.0 $cm^{-1}$ through 307.9 $cm^{-1}$; see Figure 10a,b) consist mainly of C−F and C−C−F LVM contributions, with minor contributions from the $H_2O\cdots\pi$–hole interaction at 132.6 $cm^{-1}$ and C−C/C−C−C LVMs at 263.0 $cm^{-1}$ through 307.9 $cm^{-1}$. $\omega_{\mu 8}$, $\omega_{\mu 9}$, $\omega_{\mu 23}$, and $\omega_{\mu 24}$ are 100% C1−C2−C4−C6 character. $\omega_{\mu 14}$ and $\omega_{\mu 15}$ once again have LVM contributions from the $H_2O\cdots\pi$–hole interaction of 23% and 64%, respectively. From 431.8 $cm^{-1}$ to 581.5 $cm^{-1}$, C−C and C−C−C LVMs are the major contributions, with C−F and C−C−F LVMs being minor components. After the C1−C2−C4−C6 modes at 653.5 $cm^{-1}$ through 733.3 $cm^{-1}$, $\omega_{\mu 25}$ is completely C−C−F character and $\omega_{\mu 26}$ is largely C−F character with small C−C−F and C−C contributions. Figure 10c shows $\omega_{\mu 27}$ through $\omega_{\mu 39}$ for **1**, spanning 992.0 $cm^{-1}$ through 3811.0 $cm^{-1}$.The 992.0 $cm^{-1}$ through 1143.1 $cm^{-1}$ region is C−F and C−C−F dominant, while $\omega_{\mu 31}$ at 1240 $cm^{-1}$, $\omega_{\mu 36}$ at 1639.3 $cm^{-1}$, and $\omega_{\mu 37}$ at 1639.4 $cm^{-1}$ are mainly of C−C and C−C−C character. From 1299.8 $cm^{-1}$ through 1512.0 $cm^{-1}$ a mixture of C−F, C−C−F, C−C, and C−C−C LVMs compose the $\omega_{\mu}$. At 1570.2 $cm^{-1}$ is the $H_2O$ bending mode, and the $H_2O$ stretching modes are at 3710.3 $cm^{-1}$ (symmetric) and 3811.0 $cm^{-1}$ (asymmetric). Overall, this discussion shows that the CMN feature offered by the local mode analysis provides a powerful tool for the detailed analysis of a vibrational spectrum.

## 4. Conclusions

In this work, the LVM analysis of Konkoli and Cremer was utilized to quantify strength of $\pi$–hole interactions in terms of a special local force constant $k^a$. This is the first work to quantify $\pi$–hole interactions in terms other than distance parameters $r$ and binding/dissociation energies. Given the fact that the aforementioned parameters are not reliable descriptors of bond strength, our results provide a much needed perspective on the matter. In addition to quantification of $\pi$–hole interaction strength in terms of $k^a$, this work confirms an interplay between three key factors which can influence bond strength and can be insightful for the design of materials with specific properties. The three main factors influencing $\pi$–hole interaction strength in systems **1–14** are as follows: (1) aryl-substituent effects; where F–substituents polarization of aryl C–atoms which will encourage or discourage interactions between acceptor ligands and the aryl ring. Since these effects indirectly influence the $\pi$–hole interaction by affecting the nature of the aryl ring, aryl substituent effects are the least significant of the three effects; (2) the nature of the atoms which form the aryl ring, where presence of nitrogen can substantially increase strength of the $\pi$–hole interaction, where the

more N the better; and (3) Presence of HBs and SBIs between $\pi$–hole acceptor/donor, where strength of the SBI correlates positively with strength of the $\pi$–hole interaction. HBs can have a substantial effect on strength of the $\pi$–hole interaction, depending on the directionality; where if the $\pi$–hole donor is the HB acceptor, strength of the $\pi$–hole interaction increases. Conversely, if HB donation is in the same direction as $\pi$–hole donation, the $\pi$–hole interaction will be weakened substantially. Future goals are to refine computational $\omega_\mu$ harmonic scaling factors, and to expand this research on aryl $\pi$–hole interactions to a large number of systems, including halogen anions, CO, and $OCH_3^-$ as acceptors.

**Supplementary Materials:** The following are available online at http://www.mdpi.com/2073-4352/10/7/556/s1, Figure S1: Description of the 9 possible local modes between the monomers of a dimeric system; Table S1: Description of the videos showing selected normal mode vibrations for **R2** and system **1**. The videos are uploaded as separate files; Table S2: Cartesian atomic coordinates of optimized equilibrium geometries for all model species.

**Author Contributions:** Conceptualization, S.Y., M.F., and E.K.; methodology, S.Y., M.F., Y.T., W.Z., and E.K.; validation, S.Y., M.F., Y.T., and E.K.; programming, W.Z.; formal analysis, S.Y.; investigation, S.Y.; resources, E.K.; data curation, S.Y.; writing—original draft preparation, S.Y.; writing—review and editing, M.F., and E.K.; visualization, S.Y.; supervision, E.K. and M.F.; funding acquisition, E.K. All authors have read and agreed to the published version of the manuscript.

**Funding:** This research was funded by National Science Foundation grant number CHE 1464906.

**Acknowledgments:** The authors thank SMU for providing computational resources. We thank Vytor Oliveira for helpful discussions.

**Conflicts of Interest:** The authors declare no conflicts of interest.

## Abbreviations

The following abbreviations are used in this manuscript:

| | |
|---|---|
| BE | Binding Energy |
| BSSE | Basis Set Superposition Error |
| CCP | Cage Critical Point |
| CNM | Characterization of Normal Modes |
| CT | Charge Transfer |
| DFT | Density Functional Theory |
| DE | Dissociation Energy |
| ESP | Electrostatic Potential |
| *exp* | Experimental |
| HB | Hydrogen Bond |
| lp | Lone–Pair |
| LVM | Local Vibrational Mode |
| MP2 | Møller–Plesset Perturbation Theory of Second Order |
| NBO | Natural Bond Orbital |
| NCI | Noncovalent Interaction |
| SBI | Secondary Bonding Interaction |

## References

1. Murray, J.S.; Lane, P.; Clark, T.; Riley, K.E.; Politzer, P. $\sigma$–Holes, $\pi$–Holes and Electrostatically–Driven Interactions. *J. Mol. Model.* **2011**, *18*, 541–548. [CrossRef]
2. Politzer, P.; Murray, J.S.; Clark, T. Halogen Bonding: An Electrostatically–Driven Highly Directional Noncovalent Interaction. *Phys. Chem. Chem. Phys.* **2010**, *12*, 7748. [CrossRef] [PubMed]
3. Murray, J.S.; Politzer, P. The Electrostatic Potential: An Overview. *WIREs Comput. Mol. Sci.* **2011**, *1*, 153–163. [CrossRef]
4. Politzer, P.; Murray, J.S.; Clark, T. Halogen Bonding and other $\sigma$–Hole Interactions: A Perspective. *Phys. Chem. Chem. Phys.* **2013**, *15*, 11178. [CrossRef]
5. Wang, H.; Wang, W.; Jin, W.J. $\sigma$–Hole Bond vs $\pi$–Hole Bond: A Comparison Based on Halogen Bond. *Chem. Rev.* **2016**, *116*, 5072–5104. [CrossRef]

6. Frontera, A.; Bauzá, A. Concurrent Aerogen Bonding and Lone Pair/Anion–$\pi$ Interactions in the Stability of Organoxenon Derivatives: A Combined CSD and Ab Initio Study. *Phys. Chem. Chem. Phys.* **2017**, *19*, 30063–30068. [CrossRef] [PubMed]
7. Mitra, M.; Manna, P.; Bauzá, A.; Ballester, P.; Seth, S.K.; Choudhury, S.R.; Frontera, A.; Mukhopadhyay, S. 3–Picoline Mediated Self–Assembly of M(II)−Malonate Complexes (M = Ni/Co/Mn/Mg/Zn/Cu) Assisted by Various Weak Forces Involving Lone Pair–$\pi$, $\pi$–$\pi$, and Anion$\cdots\pi$–Hole Interactions. *J. Phys. Chem. B* **2014**, *118*, 14713–14726. [CrossRef]
8. Ran, J.; Hobza, P. On the Nature of Bonding in Lone Pair$\cdots\pi$–Electron Complexes: CCSD(T)/Complete Basis Set Limit Calculations. *J. Chem. Theory Comput.* **2009**, *5*, 1180–1185. [CrossRef]
9. Foroutan-Nejad, C.; Badri, Z.; Marek, R. Multi–Center Covalency: Revisiting the Nature of Anion–$\pi$ Interactions. *Phys. Chem. Chem. Phys.* **2015**, *17*, 30670–30679. [CrossRef]
10. Mooibroek, T.J. Coordinated Nitrate Anions can be Directional $\pi$–Hole Donors in the Solid State: A CSD Study. *CrystEngComm* **2017**, *19*, 4485–4488. [CrossRef]
11. Azofra, L.M.; Alkorta, I.; Scheiner, S. Noncovalent Interactions in Dimers and Trimers of $SO_3$ and CO. *Theor. Chem. Acc.* **2014**, *133*, 1586. [CrossRef]
12. Alkorta, I.; Elguero, J.; Frontera, A. Not Only Hydrogen Bonds: Other Noncovalent Interactions. *Crystals* **2020**, *10*, 180. [CrossRef]
13. Engdahl, A.; Nelander, B. A Matrix Isolation Study of the Interaction between Water and the Aromatic $\pi$–Electron System. *J. Phys. Chem.* **1987**, *91*, 2253–2258. [CrossRef]
14. Engdahl, A.; Nelander, B. A Matrix Isolation Study of the Benzene–Water Interaction. *J. Phys. Chem.* **1985**, *89*, 2860–2864. [CrossRef]
15. Gotch, A.J.; Zwier, T.S. Multiphoton Ionization Studies of Clusters of Immiscible Liquids. I. $C_6H_6-(H_2O)_n$, n = 1, 2. *J. Chem. Phys.* **1992**, *96*, 3388–3401. [CrossRef]
16. Suzuki, S.; Green, P.G.; Bumgarner, R.E.; Dasgupta, S.; Goddard, W.A.; Blake, G.A. Benzene Forms Hydrogen Bonds with Water. *Science* **1992**, *257*, 942–945. [CrossRef]
17. Gallivan, J.P.; Dougherty, D.A. Can Lone Pairs Bind to a $\pi$ System? The Water$\cdots$Hexafluorobenzene Interaction. *Org. Lett.* **1999**, *1*, 103–106. [CrossRef]
18. Danten, Y.; Tassaing, T.; Besnard, M. On the Nature of the Water–Hexafluorobenzene Interaction. *J. Phys. Chem. A* **1999**, *103*, 3530–3534. [CrossRef]
19. Raimondi, M.; Calderoni, G.; Famulari, A.; Raimondi, L.; Cozzi, F. The Benzene/Water/Hexafluorobenzene Complex: A Computational Study. *J. Phys. Chem. A* **2003**, *107*, 772–774. [CrossRef]
20. Egli, M.; Sarkhel, S. Lone Pair–Aromatic Interactions: To Stabilize or Not to Stabilize. *Acc. Chem. Res.* **2007**, *40*, 197–205. [CrossRef]
21. Baiocco, P.; Colotti, G.; Franceschini, S.; Ilari, A. Molecular Basis of Antimony Treatment in Leishmaniasis†. *J. Med. Chem.* **2009**, *52*, 2603–2612. [CrossRef] [PubMed]
22. Hoffmann, J.M.; Sadhoe, A.K.; Mooibroek, T.J. $\pi$–Hole Interactions with Various Nitro Compounds Relevant for Medicine: DFT Calculations and Surveys of the Cambridge Structural Database (CSD) and the Protein Data Bank (PDB). *Synthesis* **2019**, *52*, 521–528. [CrossRef]
23. Egli, M.; Gessner, R.V. Stereoelectronic effects of deoxyribose O4′ on DNA conformation. *Proc. Natl. Acad. Sci. USA* **1995**, *92*, 180–184. [CrossRef]
24. Sarkhel, S.; Rich, A.; Egli, M. Water–Nucleobase "Stacking": H–$\pi$ and Lone Pair–$\pi$ Interactions in the Atomic Resolution Crystal Structure of an RNA Pseudoknot. *J. Am. Chem. Soc.* **2003**, *125*, 8998–8999. [CrossRef]
25. Belmont-Sánchez, J.C.; Ruiz-González, N.; Frontera, A.; Matilla-Hernández, A.; Castiñeiras, A.; Niclós-Gutiérrez, J. Anion–Cation Recognition Pattern, Thermal Stability and DFT–Calculations in the Crystal Structure of $H_2$dap[Cd(HEDTA)($H_2O$)] Salt ($H_2$dap = $H_2$(N3,N7)–2,6–Diaminopurinium Cation). *Crystals* **2020**, *10*, 304. [CrossRef]
26. Varadwaj, A.; Marques, H.M.; Varadwaj, P.R. Nature of Halogen–Centered Intermolecular Interactions in Crystal Growth and Design: Fluorine–Centered Interactions in Dimers in Crystalline Hexafluoropropylene as a Prototype. *J. Comput. Chem.* **2019**, *40*, 1836–1860. [CrossRef] [PubMed]
27. Bauzá, A.; Sharko, A.V.; Senchyk, G.A.; Rusanov, E.B.; Frontera, A.; Domasevitch, K.V. $\pi$–Hole Interactions at Work: Crystal Engineering with Nitro–Derivatives. *CrystEngComm* **2017**, *19*, 1933–1937. [CrossRef]
28. Bauzá, A.; Frontera, A.; Mooibroek, T.J. $NO_3^-$ Anions can Act as Lewis Acid in the Solid State. *Nat. Commun.* **2017**, *8*, 14522. [CrossRef]

29. Eliseeva, A.A.; Ivanov, D.M.; Novikov, A.S.; Kukushkin, V.Y. Recognition of the $\pi$–Hole Donor Ability of Iodopentafluorobenzene − a Conventional $\sigma$–Hole Donor for Crystal Engineering involving Halogen Bonding. *CrystEngComm* **2019**, *21*, 616–628. [CrossRef]
30. Franconetti, A.; Frontera, A.; Mooibroek, T.J. Intramolecular $\pi$–Hole Interactions with Nitro Aromatics. *CrystEngComm* **2019**, *21*, 5410–5417. [CrossRef]
31. Bauzá, A.; Frontera, A. $\sigma/\pi$–Hole Noble Gas Bonding Interactions: Insights from Theory and Experiment. *Coord. Chem. Rev.* **2020**, *404*, 213112. [CrossRef]
32. Bauzá, A.; Frontera, A. Theoretical Study on the Dual Behavior of $XeO_3$ and $XeF_4$ toward Aromatic Rings: Lone Pair–$\pi$ versus Aerogen–$\pi$ Interactions. *ChemPhysChem* **2015**, *16*, 3625–3630. [CrossRef]
33. Bauzá, A.; Frontera, A. $\pi$–Hole Aerogen Bonding Interactions. *Phys. Chem. Chem. Phys.* **2015**, *17*, 24748–24753. [CrossRef] [PubMed]
34. Bauzá, A.; Mooibroek, T.J.; Frontera, A. The Bright Future of Unconventional $\sigma/\pi$–Hole Interactions. *ChemPhysChem* **2015**, *16*, 2496–2517. [CrossRef] [PubMed]
35. Galmés, B.; Martínez, D.; Infante-Carrió, M.F.; Franconetti, A.; Frontera, A. Theoretical Ab Initio Study on Cooperativity Effects between Nitro $\pi$–Hole and Halogen Bonding Interactions. *ChemPhysChem* **2019**, *20*, 1135–1144. [CrossRef] [PubMed]
36. Galmés, B.; Franconetti, A.; Frontera, A. Nitropyridine–1–Oxides as Excellent $\pi$–Hole Donors: Interplay between $\sigma$–Hole (Halogen, Hydrogen, Triel, and Coordination Bonds) and $\pi$–Hole Interactions. *Int. J. Mol. Sci.* **2019**, *20*, 3440. [CrossRef] [PubMed]
37. Novikov, A.S.; Ivanov, D.M.; Bikbaeva, Z.M.; Bokach, N.A.; Kukushkin, V.Y. Noncovalent Interactions involving Iodofluorobenzenes: The Interplay of Halogen Bonding and Weak lp(O)$\cdots\pi$–$Hole_{arene}$ Interactions. *Cryst. Growth Des.* **2018**, *18*, 7641–7654. [CrossRef]
38. Wheeler, S.E.; Houk, K.N. Are Anion/$\pi$ Interactions Actually a Case of Simple Charge–Dipole Interactions? *J. Phys. Chem. A* **2010**, *114*, 8658–8664. [CrossRef]
39. Garau, C.; Frontera, A.; Quiñonero, D.; Russo, N.; Deyà, P.M. RI–MP2 and MPWB1K Study of $\pi$–Anion–$'$ Complexes: MPWB1K Performance and Some Additivity Aspects. *J. Chem. Theory Comput.* **2011**, *7*, 3012–3018. [CrossRef] [PubMed]
40. Politzer, P.; Murray, J.S. Electrostatics and Polarization in $\sigma$– and $\pi$–Hole Noncovalent Interactions: An Overview. *ChemPhysChem* **2020**, *21*, 579–588. [CrossRef] [PubMed]
41. Politzer, P.; Murray, J.S.; Clark, T. Explicit Inclusion of Polarizing Electric Fields in $\sigma$– and $\pi$–Hole Interactions. *J. Phys. Chem. A* **2019**, *123*, 10123–10130. [CrossRef] [PubMed]
42. Lang, T.; Li, X.; Meng, L.; Zheng, S.; Zeng, Y. The Cooperativity between the $\sigma$–Hole and $\pi$–Hole Interactions in the $ClO\cdots XONO_2$/$XONO\cdots NH_3$(X=Cl, Br, I) Complexes. *Struct. Chem.* **2014**, *26*, 213–221. [CrossRef]
43. Zierkiewicz, W.; Michalczyk, M.; Wysokiński, R.; Scheiner, S. On the Ability of Pnicogen Atoms to Engage in both $\sigma$ and $\pi$–Hole Complexes. HeteroDimers of $ZF_2C_6H_5$ (Z=P, As, Sb, Bi) and $NH_3$. *J. Mol. Model.* **2019**, *25*, 152. [CrossRef]
44. Gao, L.; Zeng, Y.; Zhang, X.; Meng, L. Comparative Studies on Group III $\sigma$–Hole and $\pi$–Hole Interactions. *J. Comput. Chem.* **2016**, *37*, 1321–1327. [CrossRef]
45. Guo, X.; Cao, L.; Li, Q.; Li, W.; Cheng, J. Competition between $\pi$–Hole Interaction and Hydrogen Bond in the Complexes of $F_2XO$ (X = C and Si) and HCN. *J. Mol. Model.* **2014**, *20*, 2493. [CrossRef]
46. Katkova, S.A.; Mikherdov, A.S.; Kinzhalov, M.A.; Novikov, A.S.; Zolotarev, A.A.; Boyarskiy, V.P.; Kukushkin, V.Y. (Isocyano Group $\pi$–Hole)$\cdots[d_{Z^2}-M^{II}]$ Interactions of (Isocyanide) $[M^{II}]$ Complexes, in which Positively Charged Metal Centers ($d^8$–M=Pt, Pd) Act as Nucleophiles. *Chem. Eur.* **2019**, *25*, 8590–8598. [CrossRef] [PubMed]
47. Liu, Z.F.; Chen, X.; Wu, W.X.; Zhang, G.Q.; Li, X.; Li, Z.Z.; Jin, W.J. 1,3,5–Trifluoro–2,4,6–triiodobenzene: A Neglected NIR Phosphor with Prolonged Lifetime by $\sigma$–Hole and $\pi$–Hole Capture. *Spectrochim. Acta A* **2020**, *224*, 117428. [CrossRef] [PubMed]
48. Varadwaj, P.R.; Varadwaj, A.; Marques, H.M. Does Chlorine in $CH_3Cl$ Behave as a Genuine Halogen Bond Donor? *Crystals* **2020**, *10*, 146. [CrossRef]
49. Rozhkov, A.V.; Krykova, M.A.; Ivanov, D.M.; Novikov, A.S.; Sinelshchikova, A.A.; Volostnykh, M.V.; Konovalov, M.A.; Grigoriev, M.S.; Gorbunova, Y.G.; Kukushkin, V.Y. Reverse Arene Sandwich Structures Based upon $\pi$–Hole$\cdots[M^{II}]$($d^8$M=Pt, Pd) Interactions, where Positively Charged Metal Centers Play the Role of a Nucleophile. *Angew. Chem. Int. Ed.* **2019**, *58*, 4164–4168. [CrossRef]

50. Prohens, R.; de Sande, D.; Font-Bardia, M.; Franconetti, A.; González, J.F.; Frontera, A. Gallic Acid Dimer As a Double $\pi$–Hole Donor: Evidence from X–ray, Theoretical Calculations, and Generalization from the Cambridge Structural Database. *Cryst. Growth Des.* **2019**, *19*, 3989–3997. [CrossRef]
51. Shukla, R.; Claiser, N.; Souhassou, M.; Lecomte, C.; Balkrishna, S.J.; Kumar, S.; Chopra, D. Exploring the Simultaneous $\sigma$–Hole/$\pi$–Hole Bonding Characteristics of a Br$\cdots\pi$ Interaction in an Ebselen Derivative via Experimental and Theoretical Electron–Density Analysis. *IUCrJ* **2018**, *5*, 647–653. [CrossRef] [PubMed]
52. Yang, F.L.; Yang, X.; Wu, R.Z.; Yan, C.X.; Yang, F.; Ye, W.; Zhang, L.W.; Zhou, P.P. Intermolecular Interactions between $\sigma$– and $\pi$–Holes of Bromopentafluorobenzene and Pyridine: Computational and Experimental Investigations. *Phys. Chem. Chem. Phys.* **2018**, *20*, 11386–11395. [CrossRef] [PubMed]
53. Yang, F.L.; Lu, K.; Yang, X.; Yan, C.X.; Wang, R.; Ye, W.; Zhou, P.P.; Yang, Z. Computational Investigations of Intermolecular Interactions between Electron–Accepting Bromo– and Iodo–Pentafluorobenzene and Electron–Donating Furan and Thiophene. *New J. Chem.* **2018**, *42*, 20101–20112. [CrossRef]
54. Zhang, J.; Hu, Q.; Li, Q.; Scheiner, S.; Liu, S. Comparison of $\sigma$–Hole and $\pi$–Hole Tetrel Bonds in Complexes of Borazine with $TH_3F$ and $F_2TO/H_2TO$ (T= C, Si, Ge). *Int. J. Quantum Chem.* **2019**, *119*, e25910. [CrossRef]
55. Zhang, Y.H.; Li, Y.L.; Yang, J.; Zhou, P.P.; Xie, K. Noncovalent Functionalization of Graphene via $\pi$–Hole$\cdots\pi$ and $\sigma$–Hole$\cdots\pi$ Interactions. *Struct. Chem.* **2019**, *31*, 97–101. [CrossRef]
56. Mikherdov, A.S.; Kinzhalov, M.A.; Novikov, A.S.; Boyarskiy, V.P.; Boyarskaya, I.A.; Avdontceva, M.S.; Kukushkin, V.Y. Ligation–Enhanced $\pi$–Hole$\cdots\pi$ Interactions Involving Isocyanides: Effect of $\pi$–Hole$\cdots\pi$ Noncovalent Bonding on Conformational Stabilization of Acyclic Diaminocarbene Ligands. *Inorg. Chem.* **2018**, *57*, 6722–6733. [CrossRef]
57. Kraka, E.; Cremer, D. Weaker Bonds with Shorter Bond Lengths. *Rev. Proc. Quim.* **2012**, *6*, 39–42. [CrossRef]
58. Setiawan, D.; Kraka, E.; Cremer, D. Hidden Bond Anomalies: The Peculiar Case of the Fluorinated Amine Chalcogenides. *J. Phys. Chem. A* **2015**, *119*, 9541–9556. [CrossRef]
59. Kraka, E.; Setiawan, D.; Cremer, D. Re–Evaluation of the Bond Length–Bond Strength Rule: The Stronger Bond Is not Always the Shorter Bond. *J. Comp. Chem.* **2015**, *37*, 130–142. [CrossRef]
60. Cremer, D.; Kraka, E. From Molecular Vibrations to Bonding, Chemical Reactions, and Reaction Mechanism. *Curr. Org. Chem.* **2010**, *14*, 1524–1560. [CrossRef]
61. Andrés, J.; Ayers, P.W.; Boto, R.A.; Carbó-Dorca, R.; Chermette, H.; Cioslowski, J.; Contreras-García, J.; Cooper, D.L.; Frenking, G.; Gatti, C.; et al. Nine questions on energy decomposition analysis. *J. Comput. Chem.* **2019**, *40*, 2248–2283. [CrossRef] [PubMed]
62. Zhao, L.; von Hopffgarten, M.; Andrada, D.M.; Frenking, G. Energy Decomposition Analysis. *WIREs Comput. Mol. Sci.* **2017**, *8*, 1–37. [CrossRef]
63. Stasyuk, O.A.; Sedlak, R.; Guerra, C.F.; Hobza, P. Comparison of the DFT-SAPT and canonical EDA Schemes for the energy decomposition of various types of noncovalent interactions. *J. Chem. Theory Comput.* **2018**, *14*, 3440–3450. [CrossRef]
64. Levine, D.S.; Head-Gordon, M. Energy decomposition analysis of single bonds within Kohn-Sham density functional theory. *Proc. Natl. Acad. Sci. USA* **2017**, *114*, 12649–12656. [CrossRef]
65. Lao, K.U.; Herbert, J.M. Energy Decomposition Analysis with a Stable Charge-Transfer Term for Interpreting Intermolecular Interactions. *J. Chem. Theory Comput.* **2016**, *12*, 2569–2582. [CrossRef] [PubMed]
66. Kraka, E.; Larsson, J.A.; Cremer, D. Generalization of the Badger Rule Based on the Use of Adiabatic Vibrational Modes. In *Computational Spectroscopy*; Grunenberg, J., Ed.; Wiley: New York, NY, USA, 2010; pp. 105–149.
67. Kalescky, R.; Zou, W.; Kraka, E.; Cremer, D. Local Vibrational Modes of the Water Dimer-Comparison of Theory and Experiment. *Chem. Phys. Lett.* **2012**, *554*, 243–247. [CrossRef]
68. Zou, W.; Kalescky, R.; Kraka, E.; Cremer, D. Relating Normal Vibrational Modes to Local Vibrational Modes: Benzene and Naphthalene. *J. Mol. Model.* **2012**, *19*, 2865–2877. [CrossRef]
69. Kalescky, R.; Kraka, E.; Cremer, D. Local Vibrational Modes of the Formic Acid Dimer–The Strength of the Double H–Bond. *Mol. Phys.* **2013**, *111*, 1497–1510. [CrossRef]
70. Wilson, E.B.; Decius, J.C.; Cross, P.C. *Molecular Vibrations*; McGraw-Hill: New York, NY, USA, 1955.
71. Woodward, L.A. *Introduction to the Theory of Molecular Vibrations and Vibrational Spectroscopy*; Oxford University Press: Oxford, UK, 1972.

72. Herzberg, G. *Molecular Spectra and Molecular Structure*, 2nd ed.; Reitell Press: New York, NY, USA, 2008; Volume I.
73. Herzberg, G. *Molecular Spectra and Molecular Structure. Volume II: Infrared and Raman Spectra of Polyatomic Molecules*; Krieger Publishing Co.: New York, NY, USA, 1991.
74. Herzberg, G.; Huber, K.P. *Molecular Spectra and Molecular Structure*; IV. Constants of Diatomic Molecules, Van Nostrand, Reinhold: New York, NY, USA, 1979.
75. Konkoli, Z.; Cremer, D. A New Way of Analyzing Vibrational Spectra. I. Derivation of Adiabatic Internal Modes. *Int. J. Quant. Chem.* **1998**, *67*, 1–9. [CrossRef]
76. Konkoli, Z.; Larsson, J.A.; Cremer, D. A New Way of Analyzing Vibrational Spectra. II. Comparison of Internal Mode Frequencies. *Int. J. Quant. Chem.* **1998**, *67*, 11–27. [CrossRef]
77. Konkoli, Z.; Cremer, D. A New Way of Analyzing Vibrational Spectra. III. Characterization of Normal Vibrational Modes in terms of Internal Vibrational Modes. *Int. J. Quant. Chem.* **1998**, *67*, 29–40. [CrossRef]
78. Konkoli, Z.; Larsson, J.A.; Cremer, D. A New Way of Analyzing Vibrational Spectra. IV. Application and Testing of Adiabatic Modes within the Concept of the Characterization of Normal Modes. *Int. J. Quant. Chem.* **1998**, *67*, 41–55. [CrossRef]
79. Cremer, D.; Larsson, J.A.; Kraka, E. New Developments in the Analysis of Vibrational Spectra on the Use of Adiabatic Internal Vibrational Modes. In *Theoretical and Computational Chemistry*; Parkanyi, C., Ed.; Elsevier: Amsterdam, The Netherlands, 1998; pp. 259–327.
80. Kraka, E.; Zou, W.; Tao, Y. Decoding chemical information from vibrational spectroscopy data: Local vibrational mode theory. *WIREs Comput. Mol. Sci.* **2020**, e1480. [CrossRef]
81. Kraka, E.; Cremer, D. Dieter Cremer's Contribution to the Field of Theoretical Chemistry. *Int. J. Quantum Chem.* **2019**, *119*, e25849. [CrossRef]
82. Zou, W.; Kalescky, R.; Kraka, E.; Cremer, D. Relating Normal Vibrational Modes to Local Vibrational Modes with the Help of an Adiabatic Connection Scheme. *J. Chem. Phys.* **2012**, *137*, 084114. [CrossRef] [PubMed]
83. Zou, W.; Cremer, D. $C_2$ in a Box: Determining its Intrinsic Bond Strength for the $X^1\ \Sigma^+_g$ Ground State. *Chem. Eur. J.* **2016**, *22*, 4087–4097. [CrossRef]
84. McKean, D.C. Individual CH bond strengths in simple organic compounds: Effects of conformation and substitution. *Chem. Soc. Rev.* **1978**, *7*, 399. [CrossRef]
85. Kalescky, R.; Kraka, E.; Cremer, D. Identification of the Strongest Bonds in Chemistry. *J. Phys. Chem. A* **2013**, *117*, 8981–8995. [CrossRef]
86. Kraka, E.; Cremer, D. Characterization of CF Bonds with Multiple–Bond Character: Bond Lengths, Stretching Force Constants, and Bond Dissociation Energies. *ChemPhysChem* **2009**, *10*, 686–698. [CrossRef]
87. Setiawan, D.; Sethio, D.; Cremer, D.; Kraka, E. From Strong to Weak NF Bonds: On the Design of a New Class of Fluorinating Agents. *Phys. Chem. Chem. Phys.* **2018**, *20*, 23913–23927. [CrossRef]
88. Sethio, D.; Lawson Daku, L.M.; Hagemann, H.; Kraka, E. Quantitative Assessment of B−B−B, B−$H_b$−B, and B−$H_t$ Bonds: From $BH_3$ to $B_{12}H_{12}{}^{2-}$. *ChemPhysChem* **2019**, *20*, 1967–1977. [CrossRef] [PubMed]
89. Oliveira, V.; Kraka, E.; Cremer, D. The Intrinsic Strength of the Halogen Bond: Electrostatic and Covalent Contributions Described by Coupled Cluster Theory. *Phys. Chem. Chem. Phys.* **2016**, *18*, 33031–33046. [CrossRef] [PubMed]
90. Oliveira, V.; Kraka, E.; Cremer, D. Quantitative Assessment of Halogen Bonding Utilizing Vibrational Spectroscopy. *Inorg. Chem.* **2016**, *56*, 488–502. [CrossRef] [PubMed]
91. Oliveira, V.; Cremer, D. Transition from Metal–Ligand Bonding to Halogen Bonding Involving a Metal as Halogen Acceptor: A Study of Cu, Ag, Au, Pt, and Hg Complexes. *Chem. Phys. Lett.* **2017**, *681*, 56–63. [CrossRef]
92. Yannacone, S.; Oliveira, V.; Verma, N.; Kraka, E. A Continuum from Halogen Bonds to Covalent Bonds: Where Do $\lambda^3$ Iodanes Fit? *Inorganics* **2019**, *7*, 47. [CrossRef]
93. Oliveira, V.; Cremer, D.; Kraka, E. The Many Facets of Chalcogen Bonding: Described by Vibrational Spectroscopy. *J. Phys. Chem. A* **2017**, *121*, 6845–6862. [CrossRef]
94. Oliveira, V.; Kraka, E. Systematic Coupled Cluster Study of Noncovalent Interactions Involving Halogens, Chalcogens, and Pnicogens. *J. Phys. Chem. A* **2017**, *121*, 9544–9556. [CrossRef]
95. Setiawan, D.; Kraka, E.; Cremer, D. Strength of the Pnicogen Bond in Complexes Involving Group VA Elements N, P, and As. *J. Phys. Chem. A* **2014**, *119*, 1642–1656. [CrossRef]

96. Setiawan, D.; Kraka, E.; Cremer, D. Description of Pnicogen Bonding with the help of Vibrational Spectroscopy - The Missing Link Between Theory and Experiment. *Chem. Phys. Lett.* **2014**, *614*, 136–142. [CrossRef]
97. Setiawan, D.; Cremer, D. Super–Pnicogen Bonding in the Radical Anion of the Fluorophosphine Dimer. *Chem. Phys. Lett.* **2016**, *662*, 182–187. [CrossRef]
98. Sethio, D.; Oliveira, V.; Kraka, E. Quantitative Assessment of Tetrel Bonding Utilizing Vibrational Spectroscopy. *Molecules* **2018**, *23*, 2763. [CrossRef] [PubMed]
99. Freindorf, M.; Kraka, E.; Cremer, D. A Comprehensive Analysis of Hydrogen Bond Interactions Based on Local Vibrational Modes. *Int. J. Quant. Chem.* **2012**, *112*, 3174–3187. [CrossRef]
100. Tao, Y.; Zou, W.; Jia, J.; Li, W.; Cremer, D. Different Ways of Hydrogen Bonding in Water - Why Does Warm Water Freeze Faster than Cold Water? *J. Chem. Theory Comput.* **2016**, *13*, 55–76. [CrossRef] [PubMed]
101. Tao, Y.; Zou, W.; Kraka, E. Strengthening of Hydrogen Bonding With the Push–Pull Effect. *Chem. Phys. Lett.* **2017**, *685*, 251–258. [CrossRef]
102. Makoś, M.Z.; Freindorf, M.; Sethio, D.; Kraka, E. New Insights into Fe–$H_2$ and Fe–$H^-$ Bonding of a [NiFe] Hydrogenase Mimic – A Local Vibrational Mode Study. *Theor. Chem. Acc.* **2019**, *138*, 76.
103. Makoś, M.Z.; Zou, W.; Freindorf, M.; Kraka, E. Metal-Ring Interactions in Actinide Sandwich Compounds: A Combined Normalized Elimination of the Small Component and Local Vibrational Mode Study. *Mol. Phys.* **2020**, in press.
104. Zhang, X.; Dai, H.; Yan, H.; Zou, W.; Cremer, D. B–H $\pi$ Interaction: A New Type of Nonclassical Hydrogen Bonding. *J. Am. Chem. Soc.* **2016**, *138*, 4334–4337. [CrossRef]
105. Zou, W.; Zhang, X.; Dai, H.; Yan, H.; Cremer, D.; Kraka, E. Description of an Unusual Hydrogen Bond Between Carborane and a Phenyl Group. *J. Organometal. Chem.* **2018**, *865*, 114–127. [CrossRef]
106. Burianova, V.K.; Bolotin, D.S.; Mikherdov, A.S.; Novikov, A.S.; Mokolokolo, P.P.; Roodt, A.; Boyarskiy, V.P.; Dar'in, D.; Krasavin, M.; Suslonov, V.V.; et al. Mechanism of Generation of *Closo*- Amidrazones. Intramol. Non- B−H$\cdots\pi$(Ph) Interact. Determ. Stab. Config. Around Amidrazone C=N Bond. *New J. Chem.* **2018**, *42*, 8693–8703. [CrossRef]
107. Alkorta, I.; Rozas, I.; Elguero, J. An Attractive Interaction between the $\pi$–Cloud of $C_6F_6$ and Electron-Donor Atoms. *J. Org. Chem.* **1997**, *62*, 4687–4691. [CrossRef]
108. Alkorta, I.; Rozas, I.; Elguero, J. Interaction of Anions with Perfluoro Aromatic Compounds. *J. Am. Chem. Soc.* **2002**, *124*, 8593–8598. [CrossRef]
109. Mascal, M.; Armstrong, A.; Bartberger, M.D. Anion-Aromatic Bonding: A Case for Anion Recognition by $\pi$–Acidic Rings. *J. Am. Chem. Soc.* **2002**, *124*, 6274–6276. [CrossRef] [PubMed]
110. Quiñonero, D.; Garau, C.; Rotger, C.; Frontera, A.; Ballester, P.; Costa, A.; Deyà, P.M. Anion–$\pi$ Interactions: Do They Exist? *Angew. Chem. Int. Ed.* **2002**, *41*, 3389–3392. [CrossRef]
111. Chai, J.D.; Head-Gordon, M. Systematic Optimization of Long–Range Corrected Hybrid Density Functionals. *J. Chem. Phys.* **2008**, *128*, 084106. [CrossRef] [PubMed]
112. Chai, J.D.; Head-Gordon, M. Long–Range Corrected Hybrid Density Functionals with Damped Atom–Atom Dispersion Corrections. *Phys. Chem. Chem. Phys.* **2008**, *10*, 6615–6620. [CrossRef] [PubMed]
113. Dunning, T.H. Gaussian Basis Sets for use in Correlated Molecular Calculations. I. The Atoms Boron through Neon and Hydrogen. *J. Chem. Phys.* **1989**, *90*, 1007–1023. [CrossRef]
114. Kendall, R.A.; Dunning, T.H.; Harrison, R.J. Electron Affinities of the First–Row Atoms Revisited. Systematic Basis Sets and Wave Functions. *J. Chem. Phys.* **1992**, *96*, 6796–6806. [CrossRef]
115. Woon, D.E.; Dunning, T.H. Gaussian Basis Sets for use in Correlated Molecular Calculations. III. The Atoms Aluminum through Argon. *J. Chem. Phys.* **1993**, *98*, 1358–1371. [CrossRef]
116. Woon, D.E.; Dunning, T.H. Gaussian Basis Sets for use in Correlated Molecular Calculations. IV. Calculation of Static Electrical Response Properties. *J. Chem. Phys.* **1994**, *100*, 2975–2988. [CrossRef]
117. Amicangelo, J.C.; Irwin, D.G.; Lee, C.J.; Romano, N.C.; Saxton, N.L. Experimental and Theoretical Characterization of a Lone Pair–$\pi$ Complex: Water–Hexafluorobenzene. *J. Phys. Chem. A* **2012**, *117*, 1336–1350. [CrossRef] [PubMed]
118. Wilson, E.B.; Decius, J.C.; Cross, P.C. *Molecular Vibrations: The Theory of Infrared and Raman Vibrational Spectra*; McGraw-Hill: New York, NY, USA, 1955.
119. Kraka, E.; Zou, W.; Filatov, M.; Tao, Y.; Grafenstein, J.; Izotov, D.; Gauss, J.; He, Y.; Wu, A.; Konkoli, Z.; et al. COLOGNE2018. 2018. Available online: http://www.smu.edu/catco (accessed on 25 March 2020).

120. Reed, A.E.; Curtiss, L.A.; Weinhold, F. Intermolecular Interactions from a Natural Bond Orbital, Donor–Acceptor Viewpoint. *Chem. Rev.* **1988**, *88*, 899–926. [CrossRef]
121. Reed, A.E.; Weinstock, R.B.; Weinhold, F. Natural Population Analysis. *J. Chem. Phys.* **1985**, *83*, 735–746. [CrossRef]
122. Reed, A.E.; Weinhold, F. Natural Localized Molecular Orbitals. *J. Chem. Phys.* **1985**, *83*, 1736–1740. [CrossRef]
123. Bader, R.F.W. A Quantum Theory of Molecular Structure and Its Applications. *Chem. Rev.* **1991**, *91*, 893–928. [CrossRef]
124. Keith, T.A. AIMAll (Version 17.11.14). 2017. Available online: aim.tkgristmill.com (accessed on 25 March 2020).
125. Frisch, M.J.; Trucks, G.W.; Schlegel, H.B.; Scuseria, G.E.; Robb, M.A.; Cheeseman, J.R.; Scalmani, G.; Barone, V.; Petersson, G.A.; Nakatsuji, H.; Li, X.; et al. *Gaussian16 Revision B.01*; Gaussian Inc.: Wallingford, CT, USA, 2016.
126. Byrd, E.F.C.; Sherrill, C.D.; Head-Gordon, M. The Theoretical Prediction of Molecular Radical Species: A Systematic Study of Equilibrium Geometries and Harmonic Vibrational Frequencies. *J. Phys. Chem. A* **2001**, *105*, 9736–9747. [CrossRef]
127. Coolidge, M.B.; Marlin, J.E.; Stewart, J.J.P. Calculations of Molecular Vibrational Frequencies using Semiempirical Methods. *J. Comput. Chem.* **1991**, *12*, 948–952. [CrossRef]
128. Galabov, B.; Yamaguchi, Y.; Remington, R.B.; Schaefer, H.F. High Level Ab Initio Quantum Mechanical Predictions of Infrared Intensities. *J. Phys. Chem. A* **2002**, *106*, 819–832. [CrossRef]
129. Halls, M.D.; Velkovski, J.; Schlegel, H.B. Harmonic Frequency Scaling Factors for Hartree–Fock, S–VWN, B–LYP, B3–LYP, B3–PW91 and MP2 with the Sadlej pVTZ Electric Property Basis Set. *Theor. Chem. Acc.* **2001**, *105*, 413–421. [CrossRef]
130. Morse, M.D. Clusters of Transition–Metal Atoms. *Chem. Rev.* **1986**, *86*, 1049–1109. [CrossRef]
131. Irikura, K.K.; Johnson, R.D.; Kacker, R.N. Uncertainties in Scaling Factors for Ab Initio Vibrational Frequencies. *J. Phys. Chem. A* **2005**, *109*, 8430–8437. [CrossRef]
132. Scott, A.P.; Radom, L. Harmonic Vibrational Frequencies: An Evaluation of Hartree–Fock, Møller–Plesset, Quadratic Configuration Interaction, Density Functional Theory, and Semiempirical Scale Factors. *J. Phys. Chem.* **1996**, *100*, 16502–16513. [CrossRef]
133. Faeder, J. A Distributed Gaussian Approach to the Vibrational Dynamics of Ar–Benzene. *J. Chem. Phys.* **1993**, *99*, 7664–7676. [CrossRef]
134. Nanayakkara, S.; Kraka, E. A New Way of Studying Chemical Reactions: A Hand-in-hand URVA and QTAIM Approach. *Phys. Chem. Chem. Phys.* **2019**, *21*, 15007–15018. [CrossRef]
135. Wei, Y.; Li, Q.; Li, W.; Cheng, J.; McDowell, S.A.C. Influence of the Protonation of Pyridine Nitrogen on Pnicogen Bonding: Competition and Cooperativity. *Phys. Chem. Chem. Phys.* **2016**, *18*, 11348–11356. [CrossRef] [PubMed]
136. Bauzá, A.; Frontera, A. Competition between Lone Pair–$\pi$, Halogen–$\pi$ and Triel Bonding Interactions Involving $BX_3$ (X=F, Cl, Br and I) Compounds: An Ab Initio Study. *Theor. Chem. Acc.* **2017**, *136*, 37. [CrossRef]
137. Vácha, R.; Marsalek, O.; Willard, A.P.; Bonthuis, D.J.; Netz, R.R.; Jungwirth, P. Charge Transfer between Water Molecules As the Possible Origin of the Observed Charging at the Surface of Pure Water. *J. Phys. Chem. Lett.* **2011**, *3*, 107–111. [CrossRef]
138. Verma, N.; Tao, Y.; Zou, W.; Chen, X.; Chen, X.; Freindorf, M.; Kraka, E. A Critical Evaluation of Vibrational Stark Effect (VSE) Probes with the Local Vibrational Mode Theory. *Sensors* **2020**, *20*, 2358. [CrossRef]